Inorganic Chemistry

Article

pubs.acs.org/IC

Synthesis, Structural Characterization, and Photophysical, Spectroelectrochemical, and Anion-Sensing Studies of Heteroleptic Ruthenium(II) Complexes Derived from 4′-Polyaromatic-Substituted Terpyridine Derivatives and 2,6-Bis(benzimidazol-2-yl)pyridine

Dinesh Maity, Shyamal Das, Sourav Mardanya, and Sujoy Baitalik*

Department of Chemistry, Inorganic Chemistry Section, Jadavpur University, Kolkata 700032, India

Supporting Information

ABSTRACT: Heteroleptic bis-tridentate ruthenium(II) complexes of composition $[(H_2pbbzim)Ru(tpy\text{-}Ar)](ClO_4)_2$, where $H_2pbbzim$ = 2,6-bis(benzimidazol-2-yl)pyridine and tpy-Ar = 4′-substituted terpyridine ligands with Ar = phenyl (**2**), 2-naphthyl (**3**), 9-anthryl (**4**), and 1-pyrenyl (**5**) groups, have been synthesized and characterized by using standard analytical and spectroscopic techniques. The X-ray crystal structures of the complexes $[(H_2pbbzim)Ru(tpy\text{-}Naph)](ClO_4)_2$ (**3**), $[(pbbzim)Ru(tpy\text{-}Naph)]\cdot(CH_3)_2CO\cdot H_2O$ (**3a**), and $[(H_2pbbzim)Ru(tpy\text{-}Py)](ClO_4)_2$ (**5**) have been determined. The absorption, steady-state, and time-resolved luminescence spectral properties of the complexes were thoroughly investigated in dichloromethane. The compounds display strong luminescence at room temperature with lifetimes (τ_2) in the range of 5.5−62 ns, depending upon the nature of the polycyclic aromatic moiety as well as the solvents. The complexes are found to undergo one reversible oxidation in the positive potential window (0 to +1.5 V) and four successive quasi-reversible reductions in the negative potential window (0 to −2.4 V). The anion-sensing properties of the receptors were thoroughly investigated in acetonitrile/dichloromethane (1/9 v/v) solutions (2×10^{-5} M) using absorption, steady-state, and time-resolved emission spectroscopic studies. ^{1}H NMR titration experiments, on the other hand, were carried out in either CD_3CN or DMSO-d_6. The anion-sensing studies revealed that the receptors act as sensors for F^-, CN^-, AcO^-, and SO_4^{2-} and to some extent for HSO_4^- and $H_2PO_4^-$. It is evident that, in the presence of excess anions, deprotonation of the imidazole N−H fragments of the receptors occurs, which is signaled by the change of color from yellow-orange to violet visible with the naked eye. From the absorption and emission titration studies the binding/equilibrium constants of the receptors with the anions have also been determined. Anion-induced lifetime quenching and/or enhancement make the receptors suitable lifetime-based sensors for selective anions. Cyclic voltammetric (CV) measurements of the compounds carried out in acetonitrile have provided evidence in favor of anion-dependent electrochemical responses with F^- and AcO^- ions. Spectroelectrochemical studies have also been carried out for both the protonated and deprotonated forms of the complexes in the range of 300−1200 nm. With successive oxidation of the Ru(II) center, replacement of MLCT bands by LMCT bands occurs gradually with observation of sharp isosbestic points in all cases.

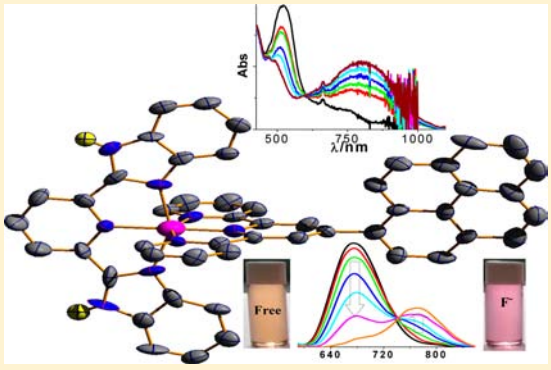

INTRODUCTION

Polypyridyl complexes of ruthenium(II) are considered as iconic building blocks for the designing of photomolecular devices because of a unique combination of their photophysical, photochemical, and electrochemical properties.[1−4] Moreover, the properties often can be tuned to a significant extent by ramification of ligand structures in the complexes.[1] The polypyridine ligands usually contain bidentate chelating sites such as 2,2′-bipyridine (bpy) and 1,10-phenanthroline (phen) and analogous tridentate chelating sites such as the variety of 2,2′:6′,2″-terpyridine (tpy) species separated by a variety of spacers to modulate size, shape, topology, and electronic effects.[1−4] The tremendous progress made in the chemistry of bipyridine and oligopyridines was initiated by the discovery of the remarkably efficient photosensitizing properties of $[Ru(bpy)_3]^{2+}$, and a number of other studies have also focused on the photoinduced electron- and energy-transfer processes of several tris-bidentate ruthenium(II) complexes.[1−4] However, the synthesis of tris(bpy)-type complexes is hampered by the mixtures of diasteromers.[5] It is well-known that this problem may be overcome by using achiral D_{2d} bis-terdentate components, particularly those substituted at the 4′-position of terpyridines.[1c,6] In contrast to $[Ru(bpy)_3]^{2+}$ type complexes, the structurally more appealing $[Ru(tpy)_2]^{2+}$ type complexes give linear rodlike assemblies when substituted at the 4′-

Received: October 15, 2012
Published: May 31, 2013

   dx.doi.org/10.1021/ic3022326 | Inorg. Chem. 2013, 52, 6820−6838

position of the tpy ligands.[6] However, usually such complexes are practically nonluminescent at room temperature and their excited-state lifetimes (τ = 0.25 ns) are also very short and therefore are the major deterrent for them to act as photosensitizers.[7] In this context, a large number of studies have been done by various research groups to design and synthesize tridentate polypyridine ligands that can produce ruthenium(II) complexes with enhanced excited-state lifetimes at room temperature. Most of the approaches aim at increasing the energy gap between the radiative ^{3}MLCT and quenching ^{3}MC states. Stabilization of the ^{3}MLCT state can be achieved by substituting the tpy ligands by electron-withdrawing groups,[8] introducing a coplanar heteroaromatic moiety,[9] incorporating organic chromophores, etc. Indeed, such approaches have produced complexes that have longer emission lifetimes in comparison to the parent compounds.[10−12] A second approach is to destabilize the ^{3}MC state by using cyclometalated ligands.[13] One can also modify the terpyridine directly, by replacing the pyridines with other heterocyclic rings to enlarge the bite angle of the tridentate ligand.[14]

We have previously reported a series of heteroleptic tridentate ruthenium(II) complexes of composition $[(H_2pbbzim)Ru(tpy\text{-}X)](PF_6)_2$, where H_2pbbzim = 2,6-bis-(benzimidazol-2-yl)pyridine and tpy-X = 4′-substituted terpyridine ligands with X = H, *p*-PhCH$_3$, *p*-PhCH$_2$Br, *p*-PhCHBr$_2$, *p*-PhCH$_2$CN, *p*-PhCH$_2$PPh$_3$Br, *p*-PhCHO groups to increase the excited-state lifetime of ruthenium(II) bis-terpyridine-type complexes.[15a] To allow fine tuning of the electronic properties, several electron-withdrawing groups have been introduced at the 4′-position of the terpyridine ligand. All of the complexes display moderately strong luminescence at room temperature with lifetimes in the range of 10−58 ns. The sub-nanosecond excited-state lifetimes of these tpy complexes are widely accepted as being due to the small energy gap between the emitting ^{3}MLCT state and the deactivating ^{3}MC level.[15] Correlations were also obtained for the Hammett σ_p parameter with their MLCT emission energies, lifetimes, redox potentials, proton NMR chemical shifts, etc.

As part of our interest in exploring new ruthenium(II) complexes of tridentate ligands with long-lived excited states at room temperature, we report herein a series of related heteroleptic bis-tridentate ruthenium(II) complexes by using 2,6-bis(benzimidazol-2-yl)pyridine (H_2pbbzim) and different 4′-aryl-substituted terpyridine derivatives (tpy-Ar). To this end we have chosen four systems, 4′-(phenyl)-2,2′:6′,2″-terpyridine (tpy-Ph), 4′-(2-naphthyl)-2,2′:6′,2″-terpyridine (tpy-Naph), 4′-(9-anthryl)-2,2′:6′,2″-terpyridine (tpy-An), and 4′-(1-pyrenyl)-2,2′:6′,2″-terpyridine (tpy-Py) (Chart 1), wherein a potentially luminescent polyaromatic moiety is directly linked to the 4′-position of a terpyridine unit via a C−C single bond, in comparison to the previously reported electron-withdrawing substituents at the 4′-position of the terpyridine moiety. It may be noted that all the 4′-substituted fused aromatic terpyridines have a significant degree of conformational flexibility along with considerable aromatic/heteroaromatic surfaces and there is a possibility to exploit interaromatic stabilizing forces as elements in the structural design.[16] Thus, it is expected that, by a change in the aromatic hydrocarbon ring, it is possible to adjust the energy and the intensity of the absorbance and at the same time tune the energy, lifetime, emission yield, and reactivity of the luminescent excited state over a wide range. Additionally, these complexes also have two imidazole NH protons which can be utilized for sensing and recognizing selective anions either via a

Chart 1

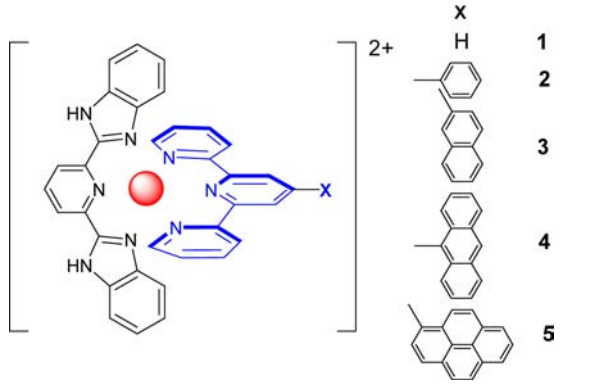

hydrogen-bonding interaction or by proton transfer. The supramolecular chemistry of anion recognition and binding is a subject of considerable contemporary research interest because of their important roles in biological, aquatic, environmental, and industrial processes.[15−25] Consequently, a great number of efforts have been directed toward designing metalloreceptors that can selectively recognize anions and act as sensors.[15−27] When the metalloreceptor is designed to function as a sensor, metal fragments can be used as reporter units for modulating a signal, usually color, fluorescence, or electrochemical potential, as a result of host−guest interactions.[18−25] Thus, the present complexes under investigation, owing to the presence of two imidazole NH protons, can be utilized for multichannel recognition of selective anions in solution. As will be seen, remarkable changes in photophysical behavior of the complexes occur on interaction with selective anions such as F^-, AcO^-, CN^-, $H_2PO_4^-$, and SO_4^{2-}. In the present work a significant effort has been given to studying lifetime-based sensing of the metalloreceptors with different anions, in comparison to previously published work. Further, spectroelectrochemical measurements in the present study provide a convenient way to follow the evolution and disappearance of different charge-transfer transitions in the absorption spectra of the complexes as the oxidation states of the metal ions change from ruthenium(II) to ruthenium(III).

EXPERIMENTAL SECTION

Materials. Reagent grade chemicals obtained from commercial sources were used as received. Solvents were purified and dried according to standard methods. 2,2′:6′,2″-Terpyridine (tpy), 2,6-pyridinedicarboxylic acid, 1,2-phenylenediamine, and the tetrabutylammonium (TBA) salts of the anions were purchased from Sigma−Aldrich. 4′-(Phenyl)-2,2′:6′,2″-terpyridine (tpy-Ph), 4′-(2-naphthyl)-2,2′:6′,2″-terpyridine (tpy-Naph), 4′-(9-anthryl)-2,2′:6′,2″-terpyridine (tpy-An), 4′-(1-pyrenyl)-2,2′:6′,2″-terpyridine (tpy-Py), and 2,6-bis-(benzimidazol-2-yl)pyridine (H_2pbbzim)[16b,28] were synthesized according to the literature procedures. $[Ru(H_2pbbzim)Cl_3]$ and $[(H_2pbbzim)Ru(tpy)](ClO_4)_2$ (**1**) were previously reported by us.[15a]

General Procedure for Preparation of the Heteroleptic Ruthenium(II) Complexes $[(H_2pbbzim)Ru(tpy\text{-}Ar)](ClO_4)_2$ (2−5). $[(H_2pbbzim)RuCl_3]$ (75 mg, 0.14 mmol) was suspended in ethylene glycol (25 mL) and heated to 100 °C with continuous stirring under nitrogen. To the suspension was added 0.15 mmol of different tpy-Ar ligands, and the reaction mixture was again heated to 180 °C for 12 h. The resulting deep red solution was cooled to room temperature, and the perchlorate salt of the complex was precipitated by pouring the solution into an aqueous solution of $NaClO_4 \cdot H_2O$ (1.0 g in 10 mL of water). The precipitate was filtered, washed several times with cold water, and then dried under vacuum. The compound was then purified

dx.doi.org/10.1021/ic3022326 | Inorg. Chem. 2013, 52, 6820−6838

by silica gel column chromatography using acetonitrile as the eluent. The eluent were reduced to about 5 mL, and to it was then added an aqueous solution of $NaClO_4 \cdot H_2O$, at which point a red microcrystalline compound deposited. The precipitate was collected and washed several times with cold water. Further purification was carried out by recrystallization of the compound from a mixture of MeCN and MeOH (1/2 v/v) in the presence of a few drops of aqueous 10^{-4} M perchloric acid.

[(H$_2$pbbzim)Ru(tpy-Ph)](ClO$_4$)$_2$·2H$_2$O (**2**). Yield: 65%. Anal. Calcd for $C_{40}H_{32}N_8Cl_2O_{10}Ru$: C, 50.21; H, 3.37; N, 11.71. Found: C, 50.19; H, 3.39; N, 11.69. ^{1}H NMR (500 MHz, DMSO-d_6, δ/ppm): 9.52 (s, 2H, H3′), 8.96 (d, 2H, J = 8.0 Hz, H3), 8.74 (d, 2H, J = 8.0 Hz, H17), 8.59 (t, 1H, J = 8.2 Hz, H16), 8.52 (d, 2H, J = 7.5 Hz, H7), 7.92 (t, 2H, J = 7.2 Hz, H4), 7.79 (t, 2H, J = 7.7 Hz, H8), 7.71(t, 1H, J = 7.5 Hz, H9), 7.63 (d, 2H, J = 8.0 Hz, H18), 7.47 (d, 2H, J = 5.5 Hz, H6), 7.27 (t, 2H, J = 7.5 Hz, H19), 7.22 (t, 2H, J = 6.5 Hz, H5) 6.99 (t, 2H, J = 7.7 Hz, H20), 6.04 (d, 2H, J = 8.5 Hz, H21). ESI-MS (positive, CH_3CN): m/z 361.06 (100%) $[(H_2pbbzim)Ru(tpy\text{-}Ph)]^{2+}$; 821.09 (8%) $[(H_2pbbzim)Ru(tpy\text{-}Ph)(ClO_4)]^+$; 721.14 (9%) [(Hpbbzim)-Ru(tpy-Ph)]$^+$. UV−vis (CH_2Cl_2; λ_{max}/nm (ε/M^{-1} cm^{-1})): 495 (13000), 402 (9700), 354 (34000), 337 (31700), 316 (41800), 286 (41550), 275 (38300).

[(H$_2$pbbzim)Ru(tpy-Naph)](ClO$_4$)$_2$·H$_2$O (**3**). Yield: 60%. Anal. Calcd for $C_{44}H_{32}N_8Cl_2O_9Ru$: C, 53.45; H, 3.26; N, 11.33. Found: C, 53.42; H, 3.29; N, 11.31. ^{1}H NMR (500 MHz, DMSO-d_6, δ/ppm): 9.65 (s, 2H, H3′), 9.14 (s, 1H, H13), 8.99 (d, 2H, J = 8.0 Hz, H3), 8.74 (d, 2H, J = 8.0 Hz, H17), 8.64 (d, 1H, J = 8.5 H7), 8.58 (t, 1H, J = 8.0 Hz, H16), 8.31 (d, 1H, J = 8.5 Hz, H8), 8.21 (d, 1H, J = 7.5 Hz, H9), 8.13 (d, 1H, J = 7.5 Hz, H12), 7.93 (t, 2H, J = 7.2 Hz, H4), 7.72−7.69 (m, 2H, 1H10 + 1H11), 7.62 (d, 2H, J = 8.5 Hz, H6), 7.47 (d, 2H, J = 5.5 Hz, H18), 7.26−7.21 (m, 4H, 2H5 + 2H19), 6.98 (t, 2H, J = 8.0, H20), 6.07 (d, 2H, J = 8.5, H21). ESI−MS (positive, CH_3CN): m/z 386.05 (100%) $[(H_2pbbzim)Ru(tpy\text{-}Naph)]^{2+}$; 871.11 (7%) $[(H_2pbbzim)Ru(tpy\text{-}Naph)(ClO_4)]^+$; 771.14 (45%) [(Hpbbzim)Ru-(tpy-Naph)]$^+$. UV−vis (CH_2Cl_2; λ_{max}/nm (ε/M^{-1} cm^{-1})): 495 (12200), 406 (3700), 354 (27750), 337 (27250), 316 (35900), 285 (32050).

[(H$_2$pbbzim)Ru(tpy-An)](ClO$_4$)$_2$·2H$_2$O (**4**). Yield: 50%. Anal. Calcd for $C_{48}H_{36}N_8Cl_2O_{10}Ru$: C, 54.55; H, 3.43; N, 10.60. Found: C, 54.54; H, 3.45; N, 10.59. ^{1}H NMR (500 MHz, DMSO-d_6, δ/ppm): 9.32 (s, 2H, H3′), 8.98 (s, 1H, H11), 8.74−8.69 (m, 4H, 2H3 + 2H17), 8.58 (t, 1H, J = 8.0 Hz, H16), 8.37 (d, 2H, J = 9.0 Hz, H10), 8.08 (d, 2H, J = 9.0 Hz, H7), 7.82−7.77 (m, 4H, 2H4 + 2H9), 7.72 (t, 2H, J = 7.2 Hz, H8), 7.66 (d, 2H, J = 8.0 Hz, H18), 7.52 (d, 2H, J = 5.5 Hz, H6), 7.34 (t, 2H, J = 7.5 Hz, H19), 7.21 (t, 2H, J = 6.5 Hz, H5), 7.17 (t, 2H, J = 7.5 Hz, H20), 6.30 (d, 2H, J = 8.0 Hz, H21). ESI-MS (positive, CH_3CN): m/z 411.07 (100%) $[(H_2pbbzim)Ru(tpy\text{-}An)]^{2+}$; 921.13 (6%) $[(H_2pbbzim)Ru(tpy\text{-}An)(ClO_4)]^+$; 821.17 (25%) [(Hpbbzim)-Ru(tpy-An)]$^+$. UV-vis (CH_2Cl_2; λ_{max}/nm (ε/M^{-1} cm^{-1})): 503 (15750), 354 (44950), 318 (59000), 276 (71900).

[(H$_2$pbbzim)Ru(tpy-Py)](ClO$_4$)$_2$·3H$_2$O (**5**). Yield: 55%. Anal. Calcd for $C_{50}H_{38}N_8Cl_2O_{11}Ru$: C, 54.65; H, 3.48; N, 10.19. Found: C, 54.64; H, 3.50; N, 10.18. ^{1}H NMR (500 MHz, DMSO-d_6, δ/ppm): 9.38 (s, 2H, H3′), 8.75 (d, 2H, J = 8.0 Hz, H3), 8.68 (d, 2H, J = 8.0 Hz, H17), 8.62−8.58 (m, 2H, 1H13 + 1H14), 8.52 (t, 1H, J = 8.0 Hz, H16), 8.45 (d, 1H, J = 9.5 Hz, H12), 8.41−8.36 (m, 3H, 1H8 + 1H9 + 1H11), 8.34−8.30 (m, 2H, 1H7 + 1H15), 8.13 (t, 1H, J = 7.5 Hz, H10), 7.79 (t, 2H, J = 7.7 Hz, H4), 7.59 (d, 2H, J = 8.0 Hz, H18), 7.44 (d, 2H, J = 5.0 Hz, H6), 7.26 (t, 2H, J = 7.5 Hz, H19), 7.15 (t, 2H, J = 6.5 Hz, H5), 7.05 (t, 2H, J = 6.5 Hz, H20), 6.17 (d, 2H, J = 8.0 Hz, H21). ESI-MS (positive, CH_3CN): m/z 423.07 (100%) $[(H_2pbbzim)Ru(tpy\text{-}Py)]^{2+}$; 945.12 (4%) $[(H_2pbbzim)Ru(tpy\text{-}Py)(ClO_4)]^+$; 845.16 (25%) [(Hpbbzim)Ru(tpy-Py)]$^+$. UV−vis (CH_2Cl_2; λ_{max}/nm (ε/M^{-1} cm^{-1})): 497 (12300), 407 (6800), 354 (30290), 339 (28600), 316 (36100), 280 (br) (26950).

Physical Measurements. Elemental (C, H, and N) analyses were performed on a Perkin-Elmer 2400II analyzer. ^{1}H NMR and {^{1}H−^{1}H} COSY spectra were obtained on a Bruker Avance DPX 500 MHz spectrometer using DMSO-d_6 solutions. Electrospray ionization mass spectra (ESI-MS) were obtained on a Micromass Qtof YA 263 mass spectrometer. Electronic absorption spectra were obtained with a Shimadzu UV 1800 spectrophotometer at room temperature. The binding studies of the receptor with different anions were carried out in acetonitrile/dichloromethane (1/9 v/v). For a typical titration experiment, 2 μL aliquots of a given anion (5.0×10^{-3} M) were added to a 2.5 mL solution of the complex (2.0×10^{-5} M) in acetonitrile/dichloromethane (1/9 v/v). TBA salts of different anions were used for titration experiments. The binding/equilibrium constants were evaluated from the absorbance data using eq 1,[29] where A_{obs} is the

$$A_{obs} = (A_0 + A_\infty K[G]_T)/(1 + K[G]_T) \quad (1)$$

observed absorbance, A_0 is the absorbance of the free receptor, A_∞ is the maximum absorbance induced by the presence of a given anionic guest, $[G]_T$ is the total concentration of the guest, and K is the binding constant of the host−guest entity.

To determine the ground-state pK_a values of the complexes, spectrophotometric titrations were carried out with a series of MeCN/aqueous buffer (3/2 v/v) solutions containing the same amount of complex (10^{-5} M) and pH adjusted in the range 2.5−12. Robinson−Britton buffers were used in the study.[30] The pH measurements were made with a Beckman Research Model pH meter. The pH meter responded reproducibly to the variation of hydrogen ion concentration and, as such, the pH meter readings were referred to as pH. The individual pK_a values were evaluated from the two segments of the spectrophotometric titration data using eq 2.

$$\mathrm{pH} = \mathrm{p}K_a - \log \frac{A - A_0}{A_f - A_0} \quad (2)$$

Steady-state emission spectra were recorded on a Perkin-Elmer LS55 fluorescence spectrophotometer. The room-temperature spectra were obtained in dichloromethane and dimethyl sulfoxide, while the spectra at 77 K were recorded in a 4/1 (v/v) ethanol/methanol glass. Photoluminescence titrations were carried out with the same sets of solutions as were used with spectrophotometry. Luminescence quantum yields were determined by a relative method using $[Ru(bpy)_3]^{2+}$ as the standard. Time-correlated single-photon-counting (TCSPC) measurements were carried out for the luminescence decay of complexes. For TCSPC measurements, the photoexcitation was carried out at 450 nm using a picosecond diode laser (IBH Nanoled-07) in an IBH Fluorocube apparatus. The lifetimes of the receptors were recorded as a function of different anions, solvents, and solution pHs. The luminescence decay data were collected on a Hamamatsu MCP photomultiplier (R3809) and were analyzed by using IBH DAS6 software.

The electrochemical measurements were carried out with a BAS Epsilon electrochemistry system. A three-electrode assembly comprising a Pt (for oxidation) or glassy-carbon (for reduction) working electrode, a Pt auxiliary electrode, and an Ag/AgCl reference electrode was used. The cyclic voltammetric (CV) and square wave voltammetric (SWV) measurements were carried out at 25 °C on an acetonitrile solution of the complex (ca. 1 mM), and the concentration of the supporting electrolyte, tetraethylammonium perchlorate (TEAP), was maintained at 0.1 M. All of the potentials reported in this study were referenced against the Ag/AgCl electrode, which under the given experimental conditions gave a value of 0.36 V for the ferrocene/ferrocenium couple. Spectroelectrochemical measurements were performed with a system consisting of a BAS Epsilon potentiostat/galvanostat, a Shimadzu 3600 UV−vis−near-IR spectrophotometer, and an optically transparent spectroelectrochemical cell specially designed by BAS.

Experimental uncertainties were as follows: absorption maxima, ±2 nm; molar absorption coefficients, 10%; emission maxima, ±5 nm; excited-state lifetimes, 10%; luminescence quantum yields, 20%; redox potentials, ±10 mV; pK_a, ±0.2.

X-ray Crystal Structure Determination. Single crystals of $[(H_2pbbzim)Ru(tpy\text{-}Naph)](ClO_4)_2$ (**3**) and [(H$_2$pbbzim)Ru(tpy-

dx.doi.org/10.1021/ic3022326 | Inorg. Chem. 2013, 52, 6820−6838

Table 1. Crystallographic Data for $[(H_2pbbzim)Ru(tpy\text{-}Naph)]^{2+}$ (3), $[(H_2pbbzim)Ru(tpy\text{-}Py)]^{2+}$ (5), and $[(pbbzim)Ru(tpy\text{-}Naph)]$ (3a)

	5	3	3a
formula	$C_{50}H_{32}N_8Cl_2O_8Ru$	$C_{44}H_{30}N_8Cl_2O_8Ru$	$C_{91}H_{60}N_{16}O_2Ru_2$
fw	1044.81	970.73	1613.71
T (K)	296(2)	293(2)	293(2)
cryst syst	monoclinic	triclinic	triclinic
space group	$P2_1/c$	$P\bar{1}$	$P\bar{1}$
a (Å)	12.3047(9)	12.596(3)	14.356(3)
b (Å)	19.7234(16)	13.643(3)	14.677(4)
c (Å)	19.5156(15)	14.164(2)	19.952(5)
α (deg)	90.00	88.326(14)	90.232(16)
β (deg)	90.466(4)	80.547(14)	105.127(15)
γ (deg)	90.00	88.024(15)	104.184(15)
V (Å^3)	4736.1(6)	2398.9(8)	3924.2(17)
D_c (g cm^{-3})	1.465	1.344	1.366
Z	4	2	2
μ (mm^{-1})	0.507	0.495	0.446
$F(000)$	2120.0	984.0	1648.0
θ range (deg)	2.21−25.00	2.18- 25.000	2.35- 25.00
no. of data/restraints/params	8308/0/622	8431/0/543	13634/0/1002
GOF on F^2	1.020	1.096	0.989
R1 ($I > 2\sigma(I)$)[a]	0.0674	0.0999	0.0752
wR2 (all data)[b]	0.1805	0.2443	0.2021
$\Delta\rho_{max}/\Delta\rho_{min}$ (e Å^{-3})	0.475/-0.471	1.596/ −1.240	1.775/ −1.653

[a] $R1(F) = \sum||F_o| - |F_c||/\sum|F_o|$. [b] $wR2(F^2) = \sum w(F_o^2 - F_c^2)^2/\sum w(F_o^2)^2$.

Py)](ClO$_4$)$_2$ (**5**) were obtained by diffusing toluene into their acetonitrile/dichloromethane (1/4 v/v) solutions, while crystals for the doubly deprotonated form [(pbbzim)Ru(tpy-Naph)]·(CH$_3$)$_2$CO·H$_2$O (**3a**) were obtained by diffusing hexane into the acetone/dichloromethane (1/1 v/v) solution of compound **3** in the presence of excess tetrabutylammonium fluoride (TBAF). X-ray diffraction data for all three crystals mounted on glass fibers and coated with perfluoropolyether oil were collected on a Bruker-AXS SMART APEX II diffractometer at 296 K equipped with a CCD detector using graphite-monochromated Mo Kα radiation (λ = 0.71073 Å). Crystallographic data and details of the structure determination are summarized in Table 1. The data were processed with SAINT,[31] and absorption corrections were made with SADABS.[31] The structures were solved by direct and Fourier methods and refined by full-matrix least squares based on F^2 using the WINGX software, which utilizes SHELX-97.[32] For the structure solution and refinement the SHELXTL software package[33] was used. The non-hydrogen atoms were refined anisotropically, while the hydrogen atoms were placed with fixed thermal parameters at idealized positions. In the case of **3**, the C20−C24 atoms were refined isotropically. The electron density map also showed the presence of some unassignable peaks, which were removed by running the program SQUEEZE.[34]

CCDC reference numbers: 905217 for **3**, 905218 for **3a**, and 905219for **5**

RESULTS AND DISCUSSION

Synthesis. The heteroleptic bis-tridentate ruthenium(II) complexes (**2**−**5**) were straightforwardly prepared in fairly good yields (50−65%) by reacting [(H$_2$pbbzim)RuCl$_3$] with the 4′-substituted terpyridine derivatives in ethylene glycol in the temperature range of 180−200 °C under nitrogen protection and then precipitating the complexes as their perchlorate salts. The complexes were then subjected to silica gel column chromatography using acetonitrile as the eluent. The complexes were finally recrystallized from an acetonitrile/methanol (1/2 v/v) mixture under mildly acidic conditions to keep the benzimidazole NH protons intact. All of the complexes were characterized by elemental (C, H, and N) analyses and ESI-MS, UV−vis, and ^{1}H NMR spectroscopic measurements, and the results are given in the Experimental Section.

The ESI mass spectra of the complexes and their simulated isotopic distribution patters are shown in Figures S1−S4 (Supporting Information). As can be seen, all the complexes show three abundant peaks in acetonitrile in their experimental ESI mass spectra. The most abundant peak ranging between m/z 361.06 for **2** and m/z 423.07 for **5** corresponds to the species $[(H_2pbbzim)Ru(tpy\text{-}Ar)]^{2+}$, as the isotopic patterns of the peak separated by 0.5 Da fit very well to the calculated isotope distribution pattern. The next peak lying in the range of m/z 721.14−845.16 is due to the species $[(Hpbbzim)Ru(tpy\text{-}Ar)]^+$, while the peak located between m/z 821.09 and 945.12 corresponds to a monopositive cation of the type $[(H_2pbbzim)Ru(tpy\text{-}Ar)(ClO_4)]^+$ (Figures S1−S4, Supporting Information).

Description of the Crystal Structures of $[(H_2pbbzim)Ru(tpy\text{-}Naph)](ClO_4)_2$ (3) and $[(H_2pbbzim)Ru(tpy\text{-}Py)](ClO_4)_2$ (5). ORTEP[35] representations of the complex cations are shown in Figure 1, and selected bond distances and angles are given in Table S1 (Supporting Information). The structures display the expected geometry, with both ligands coordinated in a tridentate meridional fashion to the ruthenium(II) center and having a distorted-octahedral geometry. Complex **3** crystallized in the triclinic form with space group $P\bar{1}$, while **5** crystallized in the monoclinic form with space group $P2_1/c$. The chelate bite angles are in the range between 77.30(3) and 80.20(3)° for **3** and between 75.00(6) and 79.50(3)° for **5**. It is to be noted that although the interligand *trans* angle made by N3−Ru−N7 (176.60(3)° for **3** and 179.80(5) for **5**) is very close to linearity, the intraligand *trans* angles (N2−Ru−N4 = 156.00(3)° and N6−Ru−N8 = 157.90(3) for **3** and N2−Ru−N4 = 153.20(5)° and N6−Ru−N8 = 158.80(3) for **5**) deviate greatly from linearity. The Ru−N bond lengths in tpy-Naph and tpy-Py are

dx.doi.org/10.1021/ic3022326 | Inorg. Chem. 2013, 52, 6820−6838

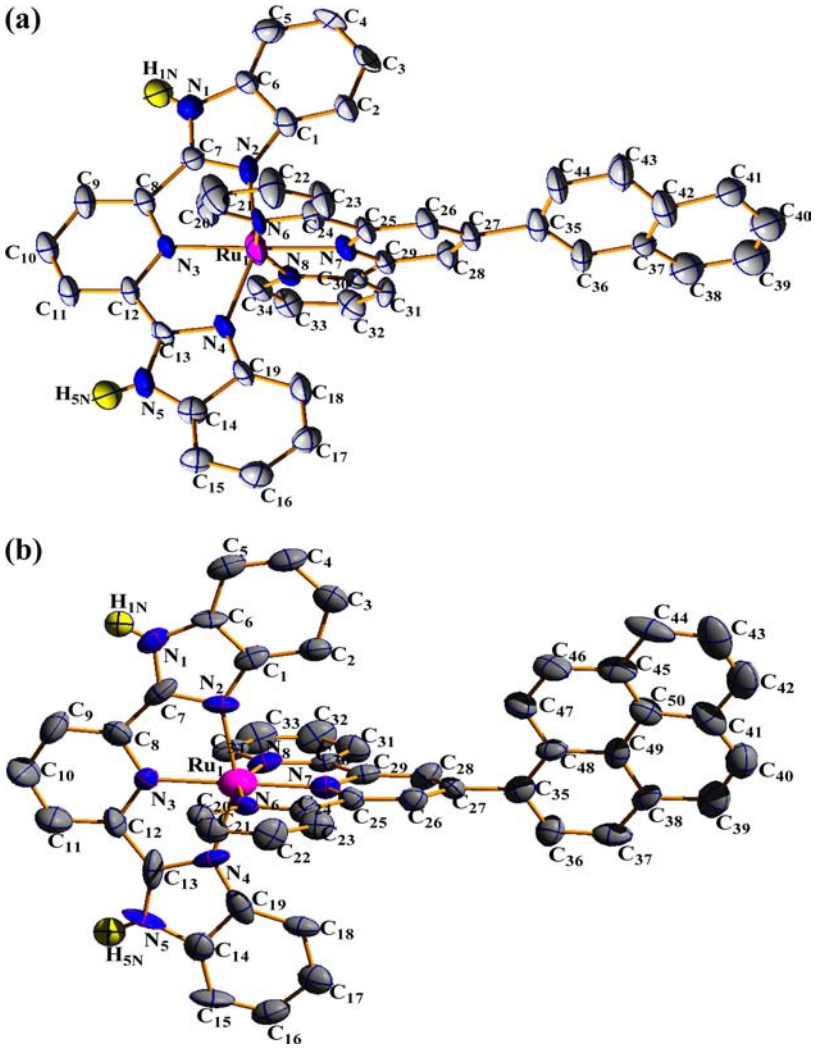

Figure 1. ORTEP[35] representations of **3** (a) and **5** (b) showing 30% probability thermal ellipsoids. Hydrogen atoms, except imidazole NH, and the ClO_4^- counteranions are omitted for clarity.

within 1.932−2.060 Å, whereas those in H_2pbbzim are relatively longer, 2.006−2.091 Å. Similar Ru−N bond distances have been previously observed in Ru(II) terpyridine type complexes.[13−15] The central Ru−N bond length is shorter than the two outer bonds to each ligand, probably because of efficient overlap of the metal t_{2g} orbital with the π^* orbitals of the central pyridyl group.

A noteworthy feature of this class of complexes is their highly twisted conformation. The X-ray crystal structures of **3** and **5** show that both the naphthyl and pyrenyl rings are not coplanar with the terpyridyl fragment but are twisted about the interannular C−C bond such that the plane of the naphthyl and pyrenyl rings makes angles of 23.47 and 71.16°, respectively, with the plane of the central pyridyl ring of the terpyridine moiety. X-ray crystal structures of 1-phenyl-, 9-anthryl-, and 1-pyrenylterpyridines have been previously determined, and it was found that the angles between the 1-phenyl, 9-anthryl, and 1-pyrenyl rings and the central pyridyl ring of the terpyridine moiety are 10.9, 74.5, and 51.6°, respectively.[6,16,36] Moreover, the dihedral angles between the central pyridine plane and the two lateral planes are different on each side of the metal center; they vary between 5.54 and 6.35° for **3** and between 1.56 and 2.16° for **5**. Thus, the twisted molecular conformation is a common feature in both these molecules.[6,37] Now it is of interest to investigate how these twisted complexes consisting of two essentially planar components pack in the solid state and what is the nature of interactions that occur. A detailed crystal structure analysis shows the occurrence of intermolecular aromatic $\pi-\pi$ and CH$-\pi$ interactions in the complexes (Figures S5−S8 and Tables S2−S4, Supporting Information).

As may be noted in the capped-stick representation of **3** (Figure S5a, Supporting Information), the two phenyl rings in the naphthyl moiety are in face-to-face alignment with the phenyl rings of another naphthyl unit. The centroid−centroid distances between these two rings are same, and the value is 3.903 Å. Again, the central pyridine ring of the benzimidazole moiety coordinated to Ru^{II} by N3 is in face-to-face alignment with the pyridine ring of another identical N3 unit. The centroid−centroid distance between these two pyridine rings is 4.055 Å. Clearly, the two naphthyl moiety and pyridine rings are involved in strong $\pi-\pi$ interactions. In the case of **5**, a similar $\pi-\pi$ interaction also occurs between the phenyl group of the benzimidazole moiety described by C1−C6 carbon atoms and a phenyl group of another pyrene moiety described by C41−C45,C50 carbon atoms and the centroid−centroid distance between the aromatic rings is 3.719° (Figure S6, Supporting Information).

dx.doi.org/10.1021/ic3022326 | *Inorg. Chem.* 2013, 52, 6820−6838

The occurrence of intermolecular CH−π interactions in **3** and **5** is also shown in Figures S5b and S7 (Supporting Information). In **3**, the H38 hydrogen atom of the naphthyl ring is in close proximity to the center of the pyridyl ring with the N8 nitrogen atom and the distance of H38 from the centroid of the pyridyl ring is 3.517 Å. Moreover, the H33 atom of a pyridyl ring with the N8 nitrogen atom is in close proximity (4.316 Å) to the center of the naphthyl ring (C37−C42). In **5**, two hydrogen atoms H22 and H32 of the two pyridyl rings are in close proximity to the centers of the phenyl rings with the C35−C38,C48,C49 and C41−C45,C50 carbon atoms, respectively. The distances of H22 and H32 from the centroids of the corresponding phenyl rings are 2.616 and 3.092 Å, respectively. Further, the H44 hydrogen atom of the pyrene ring is simultaneously close to both the center of the benzene ring (C1−C6) of the benzimidazole moiety and the π cloud of the pyridyl ring formed by N6,C20−C24 and the corresponding distances are 3.963 and 3.407 Å, respectively. It is of interest to note that the perchlorate anions are located between the planes containing the complex cation chains (Figures S5c and S8, Supporting Information) and form short contacts to protons in the planes above and below (H- - -O contacts in the range of 2.278−2.677 Å for **3** and between 2.387 and 2.711 Å for **5**).

Proton NMR Spectra. ^{1}H and {^{1}H−^{1}H} COSY NMR spectra for complexes **1**−**5** were recorded in DMSO-d_6 at room temperature to confirm the molecular structures of the compounds in solution, and their chemical shift values are given in the Experimental Section. The ^{1}H NMR spectra for complexes **2**−**5** are shown in Figure S9 (Supporting Information). The ^{1}H NMR spectra of the complexes are complicated due to the presence of the two different types of ligands. The spectral assignments of the complexes have been made with the help of their {^{1}H−^{1}H} COSY spectra (Figures S10 and S11, Supporting Information), by noting the relative areas of the peaks and taking into consideration the usual ranges of J values for H_2pbbzim and tpy-Ar.[15] The assignments made for the observed chemical shifts, according to the numbering scheme (Scheme 1), are given in Table S5 (Supporting Information). The X-ray crystal structures described above illustrate that the polyaromatic group has indeed been effective at aggregating the discrete ruthenium(II) terpyridyl complexes into polymeric chains in the solid state. In order to check whether aggregation occurs in the solution state, serial NMR dilution experiments were performed on the complexes in DMSO-d_6 solutions, starting from a saturated solution in DMSO-d_6. It is of interest to note that the positions and appearances of the proton resonances were unaltered, implying that the aromatic hydrocarbon moiety does not cause aggregation in solution.

Scheme 1

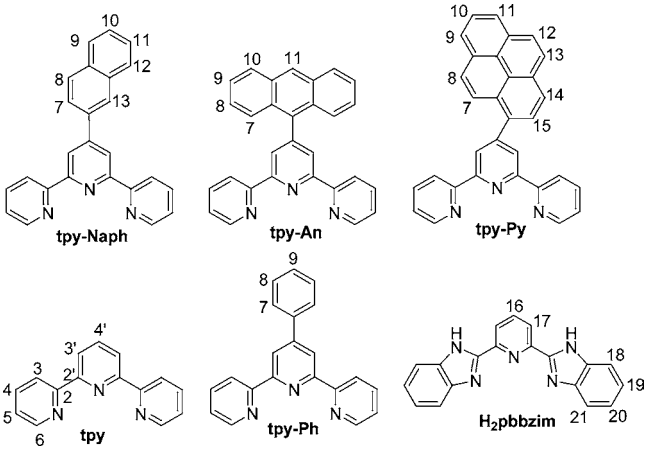

Absorption Spectra. The UV−vis absorption spectra of complexes **1**−**5** are shown in Figure 2, and their absorption

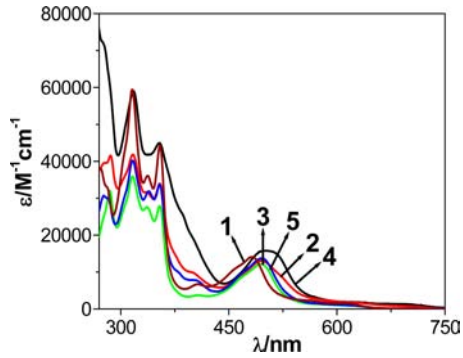

Figure 2. Absorption spectra of **1**−**5** at room temperature in dichloromethane.

maxima and molar extinction coefficients (ε) are given in Table 2, which also contains data for reference mononuclear model complexes. The absorption spectra of the complexes are of similar type, showing a number of bands in the UV−vis region, and the spectra can be regarded as the sum of the spectra of $[Ru(tpy)_2]^{2+}$, $[Ru(H_2pbbzim)_2]^{2+}$, and the polyaromatic moieties (benzene, naphthalene, anthracene, and pyrene). Assignments of the bands were made by comparing with the spectra of $[Ru(tpy)_2]^{2+}$, $[Ru(H_2pbbzim)_2]^{2+}$, and related bis-tridentate Ru(II) complexes.[1−3,6,15] Thus, in the UV region, the spectra are dominated by the π−π* transitions of the tpy, H_2pbbzim, and polyaromatic moieties. All of the complexes exhibit a fairly strong and relatively broad absorption peak in the visible range between 484 and 503 nm (ε = 12200−15750 M^{-1} cm^{-1}), which can be assigned as $^1[Ru^{II}(d\pi)^6] \rightarrow {}^1[Ru^{II}(d\pi)^5 tpy\text{-}Ar(\pi^*)^1]$ and $^1[Ru^{II}(d\pi)^6] \rightarrow {}^1[Ru^{II}(d\pi)^5 H_2pbbzim(\pi^*)^1]$. For each of the heteroleptic complexes, two distinct MLCT bands might be expected; however, as a result of the broad nature of the bands and their relatively small wavelength separation, a single broad peak is observed centered between the expected positions of the two bands. It is to be noted that the absorption spectra of the complexes also contain a low-energy shoulder in the range of 600−700 nm. This band may also arise from $^1[Ru^{II}(d\pi)^6] \rightarrow {}^3[Ru^{II}(d\pi)^5 tpy\text{-}Ar(\pi^*)^1]$ transitions.[38] It is also of interest to note that the lowest energy ^{1}MLCT absorption band for **2**−**5** is shifted to longer wavelength in comparison to the parent $[Ru(tpy)_2]^{2+}$ (474 nm) and $[Ru(H_2pbbzim)_2]^{2+}$ (475 nm) complexes, due to the extended delocalization of the tpy-Ar moiety, as expected.[1c,39] Dilution experiments performed on the complexes in acetonitrile solutions of the complexes over the 10^{-3}−10^{-5} M concentration range revealed no changes in peak maxima, shape, or extinction coefficients, which again is consistent with an absence of solution aggregation and is in agreement with the NMR observations.

Luminescence Spectra. The steady-state luminescence spectra of the compounds in dichloromethane solution at room temperature, in EtOH/MeOH (4/1 v/v) glass at 77 K and in

dx.doi.org/10.1021/ic3022326 | Inorg. Chem. 2013, 52, 6820−6838

Table 2. Spectroscopic and Photophysical Data for Complexes 1−5 in Dichloromethane Solutions

compd	absorption λ_{max}/nm (ε/M^{-1} cm^{-1})	luminescence at 298 K[a] λ_{max}/nm	τ/ns	$\Phi/10^{-3}$	$k_r/10^5$ s^{-1}	$k_{nr}/10^7$ s^{-1}	luminescence at 77 K[b] λ_{max}/nm	Φ
1	484 (14000), 406 (sh) (6700), 354 (44300), 337 (36000), 315 (59400), 282 (sh) (32000) 272 (38000)	660	1.5, 7	0.74	4.92, 1.05	66, 14	654	0.17
2	495 (13000), 402 (9700), 354 (34000), 337 (31700), 316 (41800), 286 (41550), 275 (sh) (38300)	671	1.8, 5.5	1.95	10.83, 3.54	55, 18	663	0.19
3	495 (12200), 406 (sh) (3700), 354 (27750), 337 (sh) (27250 316 (sh) (35900), 285 (32050)	680	2, 15	2.1	10.51, 1.41	50, 6.61	668	0.20
4	503 (br) (15750), 354 (44950), 318 (59000), 276 (sh) (71900)	677	1.9, 6.5	0.85	4.47, 1.33	52, 15	700	0.18
5	497 (12300), 407 (sh) (6800), 354 (30290), 339 (28600), 316 (36100), 280 (br) (26950)	673	2.2, 16	2.0	1.25, 9.12	45.35, 6.25	668	0.21
$[Ru(tpy)_2]^{2+}$[c]	474 (10400)	629	0.25	≤0.05	0.04	90.9	598	
$[Ru(tpy\text{-}PhCH_3)_2]^{2+}$[d]	490 (28000)	640	<5.0	≤0.03			628, 681 (sh)	
$[Ru(H_2pbbzim)_2]^{2+}$[e]	475 (17400)							

[a]In DCM (**1**−**5**) and CH_3CN (**6**−**8**). [b]MeOH/EtOH (1/4) glass. [c]Reference 1c. [d]Reference 1c. [e]Reference 39.

the solid powder state, are displayed in Figure 3. A summary of the photophysical data (emission maxima, quantum yield (Φ), lifetime (τ), etc.) of the complexes together with the data available for the reference mononuclear compounds is given in Table 2. All five Ru(II) complexes, on excitation at their MLCT band, exhibit one broad luminescent band, which lies between 660 (**1**) and 680 nm (**3**) in solution at 298 K, between 665 (**2**) and 707 nm (**5**) in the solid state at 298 K, and between 654 (**1**) and 700 nm (**4**) at 77 K. On the basis of extensive investigations performed on $[Ru(tpy)_2]^{2+}$ and related complexes, it can be concluded that these bands have the characteristics of emission from the ^{3}MLCT excited state, which corresponds to a spin-forbidden $Ru^{II}(d\pi) \rightarrow$ tpy-Ar(π^*) transition.[1−3,6,15] The most striking features of this class of Ru(II) compounds are that they are luminescent at room temperature in fluid solutions even though the parents $[Ru(tpy)_2]^{2+}$ [1c] and $[Ru(H_2pbbzim)_2]^{2+}$ [39] are practically nonluminescent. Luminescence lifetimes of all of the complexes were measured in dichloromethane as well as dimethyl sulfoxide at room temperature, and the decay profiles of the complexes are presented in Figure S12 (Supporting Information). The room-temperature lifetimes (τ_2) of the complexes, which lie between 5.5 (**2**) and 62 ns (**3**), are significantly greater than that of the parent $Ru(tpy)_2$ (0.25 ns). It is interesting to note that the enhanced luminescence properties of the complexes have been achieved without lowering the excited-state energy significantly. On passing from fluid solution to frozen glass, the emission maxima gets blue-shifted with a significant increase of emission intensity and quantum yield, typical of the ^{3}MLCT emitters.[1,6,15] It is to be noted that the emission maximum of the complexes is also shifted to longer wavelength in comparison to that of the parent $[Ru(tpy)_2]^{2+}$ at both room temperature and 77 K. Thus, the luminescence behaviors of the complexes are in the same line as their absorption behavior.

The zero−zero excitation energy (E_{00}) values of the ^{3}MLCT excited states of the complexes (**1**−**5**) were estimated from the energy of the emission maximum at 77 K. The E_{00} values thus estimated are 1.89 eV for $[(H_2pbbzim)Ru(tpy)]^{2+}$ (**1**), 1.87 eV for $[(H_2pbbzim)Ru(tpy\text{-}Ph)]^{2+}$ (**2**), 1.85 eV for $[(H_2pbbzim)\text{-}Ru(tpy\text{-}Naph)]^{2+}$ (**3**), 1.77 eV for $[(H_2pbbzim)Ru(tpy\text{-}An)]^{2+}$ (**4**), and 1.85 eV for $[(H_2pbbzim)Ru(tpy\text{-}Py)]^{2+}$ (**5**). At 77 K, each spectrum displays a well-defined vibronic progression in the lower energy region with spacings of ∼1281 cm^{-1} for **1**, ∼1267 cm^{-1} for **2**, ∼1268 cm^{-1} for **3**, ∼1312 cm^{-1} for **4**, and ∼1324 cm^{-1} for **5**, which are similar to those reported for

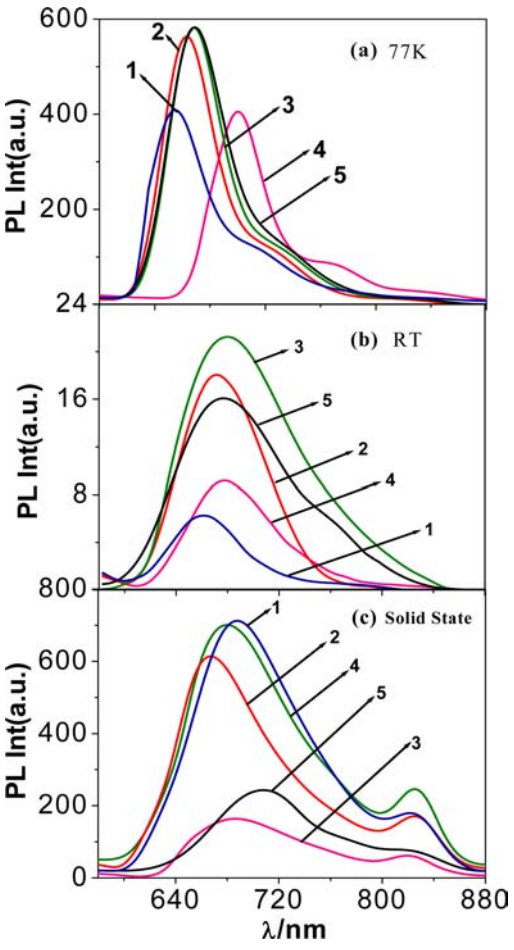

Figure 3. Photoluminescence spectra of **1**−**5** at 77 K in methanol/ethanol (1/4 v/v) glass (a), at room temperature in dichloromethane (b), and in the solid powder state (c).

dx.doi.org/10.1021/ic3022326 | Inorg. Chem. 2013, 52, 6820−6838

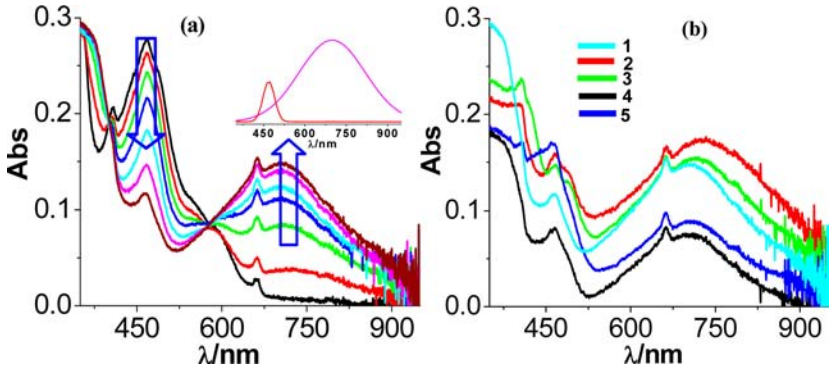

Figure 4. (a) Spectroelectrochemical changes during the oxidation of $[(H_2pbbzim)Ru(tpy)]^{2+}$ (**1**). The inset shows the deconvoluted MLCT and LMCT bands. (b) Spectra obtained after complete oxidation of complexes **1**−**5**.

$[Ru(tpy)_2]^{2+}$ and the other mono-tpy complexes of Ru(II) and can be attributed to aromatic stretching vibrations of the ligands.[38,40]

It has been observed from the reported literature data that while the majority of the ruthenium(II) complexes of bipyridyl ligands exhibit characteristic red luminescence from the ^{3}MLCT state, for the ruthenium(II) complex of terpyridyl ligands, this state is quenched by a close-lying metal-centered (^{3}MC) level and room-temperature emission is not observed.[1−3,6] The small energy difference between MLCT and MC states in Ru(II) tridentate polypyridine complexes is due to an ill-fitted octahedral arrangement, which in turn is responsible for the poor room-temperature luminescence properties of $Ru(tpy)_2$-type complexes.[6−10] Previously, we have shown that addition of simple donor and acceptor substituents at the 4′-position of tpy ligand alters the relative energies of these states and by appropriate combinations of different tridentate ligands we were able to modulate the luminescent behavior of the complexes in a predictable fashion.[15] For aryl substituents the situation is complicated by the potential for interaryl twisting in the ground and excited states.[6,37] It was reported that substitution of phenyl and *p*-tolyl groups at the 4′-position of the tpy gives the Ru(II) complexes $[Ru(Ph\text{-}tpy)_2]^{2+}$ and $[Ru(p\text{-}tolyl\text{-}tpy)_2]^{2+}$, which have room-temperature luminescence lifetimes of approximately 4 and 0.95 ns, respectively.[8] The ^{3}MLCT states in these complexes are stabilized by the phenyl or *p*-tolyl substituent to a greater extent than the ^{1}MLCT state, an effect that has been observed in a number of similar systems.[6d,41,42] In the ground state, the phenyl ring twists away from the central pyridine ring due to unfavorable steric interactions between the hydrogens ortho to the interannular C−C bond of terpyridine. In the excited state, there is a change in the dihedral angle between the phenyl ring and the central pyridine ring to give a coplanar arrangement. Consequently, the ^{3}MLCT excited state is more stabilized by extended electron delocalization than the ground state.[6d] Similar to the case for these systems, our complexes exhibit moderately strong red luminescence. Moreover, we used different polyaromatic moieties such as naphthalene, anthracene, pyrene, etc. to fine tune the ^{3}MLCT energy of the complexes (Chart 1). In the present systems, the energy of the MC level being considered to be constant, the MLCT emitting level is decreased in energy by modulating the electronic influence of the polyaromatic hydrocarbon moiety on the 4′-position of terpyridine, thereby reducing the efficiency of the MLCT to MC surface-crossing pathway. All of the heteroleptic complexes exhibit biexponential radiative decay, with initial room-temperature luminescence lifetimes in the range of 1−13 ns followed by a relatively longer lived component with excited-state lifetime ranging between 5.5 and 16 ns in dichloromethane and between 31 and 62 ns in dimethyl sulfoxide (Figure S12, Supporting Information). The first component may be attributed to the ^{3}MLCT state based on the tpy-Ar unit, and the second component probably arises from the equilibrium with the triplet state of the fused aromatic moiety which repopulates the ^{3}MLCT state after the initial emission.[9,43]

Electrochemical Properties. The electrochemical characteristics of complexes **1**−**5** have been examined by cyclic voltammetry (CV) and square wave voltammetry (SWV) in CH_3CN solutions, and the relevant electrochemical data are given in Table S6 (Supporting Information), together with the results available for the reference mononuclear species. The complexes are found to undergo one reversible oxidation in the positive potential window (0 to +1.5 V) and several successive quasi-reversible or irreversible reductions in the negative potential window (0 to −2.4 V) (Figures S13 and S14, Supporting Information). In ruthenium(II) polypyridyl complexes the highest occupied molecular orbital (HOMO) is normally localized on the Ru^{II} center and oxidative processes are therefore metal-based, whereas the lowest unoccupied molecular orbital (LUMO) is usually ligand-based and the reduction processes are therefore ligand-centered, in agreement with literature data and the reversibility of most of the processes.[1−3,6,15,44] Thus, the oxidation in the range of 1.08−1.11 V for the complexes has been assigned as a Ru^{II}/Ru^{III} process, while the reductions in the negative potential window are due to the substituted terpyridine rings and the benzimidazole moiety. It is to be noted that the Ru^{II}/Ru^{III} oxidation potentials of the complexes are significantly lower than that of $[Ru(tpy/tpy\text{-}PhCH_3)_2]^{2+}$.[1d] This is in agreement with the spectroscopic data already noted in the previous sections. The first reduction process observed between −1.43 and −1.48 V and the second reduction observed between −1.78 and −1.91 V in all of the heteroleptic complexes $[(H_2pbbzim)Ru(tpy\text{-}Ar)]^{2+}$ can be assigned as tpy-Ar centered by comparing the reduction potentials with those of free tpy-Ar ligands (between −1.70 and −2.04 V) as well as those of other tpy-based ruthenium(II) complexes. The reduction processes occurring between −2.07 and −2.09 V, on the other hand, may be due to $H_2pbbzim/H_2pbbzim^-$ ligand-centered processes.

Spectroelectrochemistry. Spectroelectrochemical measurements were carried out for compounds **1**−**5** in acetonitrile at room temperature over the spectral range 300−1000 nm. The spectral changes that take place for **1**−**5** are shown in

dx.doi.org/10.1021/ic3022326 | *Inorg. Chem.* 2013, 52, 6820−6838

Figure 4 and Figure S15 (Supporting Information). Figure 4a shows the spectral changes that occur during the electrochemical oxidation of **1** at 1.09 V. The intensity of the broad MLCT band of **1** at 468 diminishes gradually along with the growth of a new broad band around 700 nm. During electrochemical oxidation the successive absorption curves pass through an isosbestic point at 580 nm. Deconvolution of the spectral features between 350 and 1000 (inset to Figure 4a) gives rise to two peaks at 467 nm (ν = 10683 cm^{-1}, ε = 6655 M^{-1} cm^{-1}) and 702 nm (ν = 7117 cm^{-1}, ε = 14000 M^{-1} cm^{-1}). The overall changes in the spectral profiles of the other complexes (**2**–**5**) are basically similar to that of **1** with distinct changes in their absorption spectral profiles and clear isosbestic points (Figure S15, Supporting Information). It may be noted that, in all the cases, the metal to ligand charge transfer (MLCT) band gradually disappears at the expense of the evolution of a ligand to metal charge transfer (tpy-Ar → Ru^{III} LMCT) band at considerably higher wavelengths ranging between 702 and 725 nm (Table S7, Supporting Information). The presence of a clean isosbestic point in the absorption spectral profiles during the electrochemical oxidation indicates that only a single equilibrium exists between two species, namely the Ru^{II} and Ru^{III} forms of the complexes.

Anion-Sensing Studies of the Metalloreceptors through Different Channels. The sensing ability of the metalloreceptors toward various anions was studied qualitatively by visual examination of the anion-induced color changes of the metalloreceptors in acetonitrile/dichloromethane (1/9 v/v) solutions (2×10^{-5} M) before and after the addition of the anions as their TBA salts. The photographs in Figure 5 and

Figure 5. Color changes that occur when the solutions of **1** are treated with various anions as their tetrabutylammonium (TBA) salts.

Figure S16 (Supporting Information) show the significant color changes of the metalloreceptors in the presence of F^-, CN^-, AcO^-, and SO_4^{2-} in contrast to other anions such as Cl^-, Br^-, I^-, NO_3^-, and ClO_4^-. The anion-specific response makes the complexes colorimetric sensors principally for F^-, CN^-, AcO^-, and SO_4^{2-}.

The sensing of the receptors (**1**–**5**) toward anions was studied through UV–vis absorption spectroscopy. Figure 6 shows that the typical MLCT peak at 490 nm remains practically unchanged upon addition of 4 equiv of Cl^-, Br^-, I^-, NO_3^-, and ClO_4^- ions to 2.0×10^{-5} M solutions of $[(H_2pbbzim)Ru(tpy\text{-}Naph)](ClO_4)_2$ (**3**). On the other hand, following the addition of 4 equiv of F^-, CN^-, AcO^-, and SO_4^{2-}, the MLCT band is red-shifted to 540 nm, indicating that strong interactions occur between the receptor and anions. On addition of HSO_4^- and $H_2PO_4^-$, the MLCT band of complex is initially red-shifted to some extent, but the addition of an excess of these anions leads to the precipitation of the resulting complex. It may be mentioned that the extent of the shift in the case of HSO_4^- is much less in comparison to $H_2PO_4^-$. Similar red shifts of MLCT bands in the other complexes also occur on addition of these anions (Figures S17 and S18, Supporting Information). These observations are in consonance with the visual changes already noted in Figure 5 and Figure S16 (Supporting Information). The red shift of the MLCT bands can be attributed to the anion-induced deprotonation of the NH protons of the imidazole moieties in the complexes, which increases the electron density at the metal center, leading to lowering of the MLCT band energies.[15a,25,27d,45]

UV–vis absorption titrations of the receptors were carried out systematically with various anions to get a quantitative insight into sensor–anion interactions. Typical spectral changes that occur for **3** as a function of F^- are shown in Figure 7a,b. As can be seen in Figure 7a, the intensity of the MLCT peak at 490 nm decreased upon incremental addition of F^- up to 1 equiv and at its expense a new peak at 510 nm appeared with two isosbestic points at 504 and 430 nm. Continuous addition of F^- up to 4 equiv induces the MLCT peak at 510 nm to decrease in intensity further and a new absorption band at 540 nm progressively develops (Figure 7b). The final solution turns violet. After that, the change in the absorption spectral profile is negligible. The spectral changes that occur for other complexes as a function of F^-, AcO^-, CN^-, and SO_4^{2-} [46] ions are shown in Figures S19–S27 (Supporting Information). On close inspection of the changes in the absorption spectral profiles with the incremental addition of anions, the occurrence of two successive reaction equilibria becomes evident in all of the cases. In the first case, spectral saturation occurs with the addition of 1 equiv of anion (shown in the inset of Figure 7 and Figures S19–S27, Supporting Information), suggesting a 1/1 receptor/anion interaction, while for the attainment of the second equilibrium process an excess of the anion is required. The absorption spectral profiles of all the complexes are

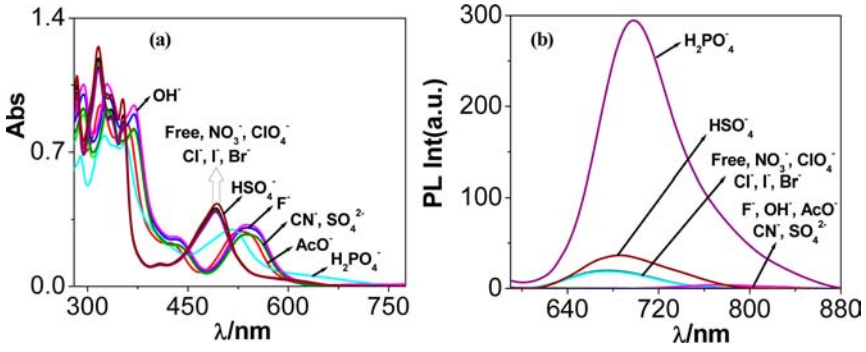

Figure 6. Changes in UV–vis absorption (a) and luminescence (b) spectra of the receptor **3** in acetonitrile/dichloromethane (1/9 v/v) solution upon the addition of different anions as TBA salts.

dx.doi.org/10.1021/ic3022326 | Inorg. Chem. 2013, 52, 6820–6838

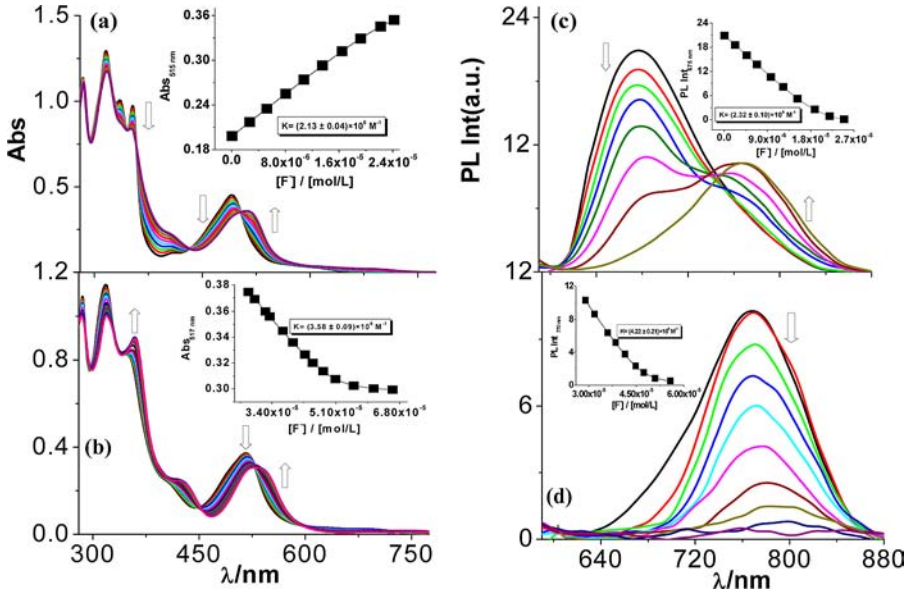

Figure 7. Changes in absorption ((a) 0−1 equiv) and (b) 1−4 equiv) and photoluminescence ((c) 0−1 equiv and (d) 1−4 equiv) spectra of **3** in acetonitrile/dichloromethane (1/9 v/v) solution (2.0×10^{-5} M) upon incremental addition of F^- ion (5.0×10^{-3} M). The insets show the fit of the experimental absorbance (a and b) and luminescence (c and d) data to a 1/1 binding profile.

Table 3. Equilibrium/Binding Constants[a,b] ($K/10^6$ M^{-1}) for 1−5 toward Various Anions in Acetonitrile/Dichloromethane (1/9 v/v) at 298 K

	1		2		3		4		5	
anion	K_1	K_2	K_1	K_2	K_1	K_2	K_1	K_2	K_1	K_2
From Absorption Spectra										
F^-	2.07	1.82	3.56	2.92	2.13	3.58	4.39	3.57	3.73	4.09
CN^-	4.31	4.56	3.64	3.31	4.66	3.92	4.63	4.03	3.94	6.28
AcO^-	1.66	1.42	2.18	2.79	1.48	3.41	1.88	2.93	2.30	3.62
SO_4^{2-}	1.34	1.24	NA[c]	NA	1.39	3.27	1.37	2.83	3.38	2.56
$H_2PO_4^-$	1.14	NA	1.98	NA	1.29	NA	1.19	NA	2.01	NA
From Emission Spectra										
F^-	2.05	1.71	2.74	2.80	2.32	4.22	2.38	3.82	2.26	3.36
CN^-	2.36	3.51	3.66	3.76	3.96	4.47	3.11	5.04	NA	NA
AcO^-	1.16	1.12	2.58	1.95	1.82	3.55	2.15	2.49	2.14	2.61
SO_4^{2-}	1.19	1.08	NA	NA	1.12	3.40	NA	NA	NA	NA
$H_2PO_4^-$	1.01	NA	NA	NA	NA	NA	NA	NA	NA	NA

[a] *tert*-Butyl salts of the respective anions were used for the studies. [b] Estimated errors were <15%. [c] Not applicable.

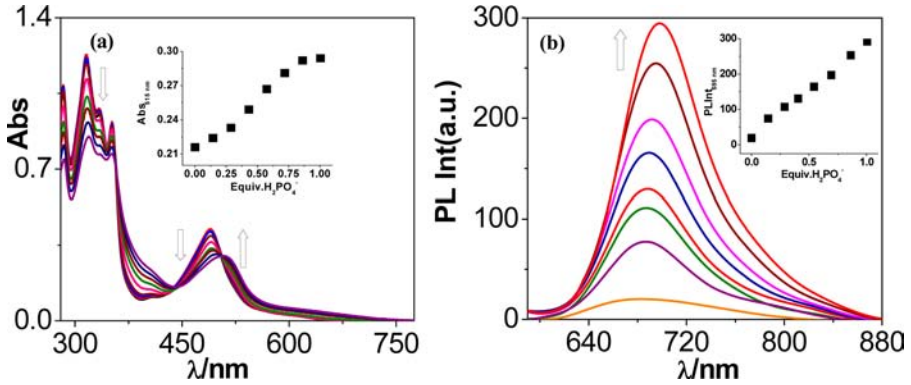

Figure 8. Changes in absorption (a) and photoluminescence (b) spectra of **3** in acetonitrile/dichloromethane (1/9 v/v) solution (2.0×10^{-5} M) upon the addition of $H_2PO_4^-$ ion (5.0×10^{-3} M). The insets show the change in absorbance (a) and luminescence intensity (b) as a function of the amount of $H_2PO_4^-$ ion.

basically similar except for the position and intensity of the band maxima and follow the same trends with the increasing concentration of the said anions (Figures S19−S27, Supporting Information). By using eq 1 the equilibrium constants K for

dx.doi.org/10.1021/ic3022326 | *Inorg. Chem.* 2013, 52, 6820−6838

receptor−anion interaction were calculated and the values are given in Table 3.[47]

Figure 8a shows the changes in the absorption spectral profile of **3** toward $H_2PO_4^-$ ion. During the process of adding 1 equiv of $H_2PO_4^-$ to a solution of **3**, the intensity of the MLCT peak at 490 nm gradually decreases, while a new band at 510 nm forms. Further addition of $H_2PO_4^-$ ion gives rise to no detectable change in the absorption spectra of **3** and thereafter leads to the precipitation of the resulting complex. The appearance of two sharp isosbestic points at 505 and 440 nm in the titration profile indicates that only two species coexist at the equilibrium and form a 1/1 stoichiometry between **3** and $H_2PO_4^-$. The spectral patterns of the other receptors toward $H_2PO_4^-$ ion are almost similar to that of **3** (Figure S28, Supporting Information). The spectral changes that occur for the receptors in the presence of HSO_4^- are shown in Figures S29−S31 (Supporting Information). It is seen that up to 1 equiv very small changes occur and further addition of HSO_4^- beyond 1 equiv gives rise to the precipitation of the resulting complex, similar to the case for $H_2PO_4^-$.

All of the complexes in the present investigation exhibit moderately strong luminescence at room temperature which can provide more than one optical signal for sensing studies. Figure 6b shows that the typical emission intensity of the band at 675 nm for **3** undergoes a nominal change with the addition of Cl^-, Br^-, I^-, NO_3^-, and ClO_4^- ions. On the other hand, with the 4-fold addition of F^-, AcO^-, CN^-, and SO_4^{2-} ions the emission intensity becomes significantly quenched with a consequent red shift of the emission maximum. In contrast, with HSO_4^- and $H_2PO_4^-$ significant augmentation of luminescence intensity occurs. Photoluminescence titrations of the receptors with various anions have been carried out in the same way as already described for spectrophotometric measurements. The quenching of luminescence intensity on incremental addition of F^- ions to the solution of **3** is presented in Figure 7c,d. Figure 8, on the other hand, shows the enhancement of the luminescence intensity of **3** as a function of $H_2PO_4^-$ ion. The emission spectral changes that occur for other complexes as a function of F^-, AcO^-, CN^-, SO_4^{2-}, HSO_4^-, and $H_2PO_4^-$ ions are shown in Figures S19−S31 (Supporting Information). It is of interest to note that, in contrast to F^-, AcO^-, CN^-, and SO_4^{2-}, enhancement of the emission intensity occurs in all of the complexes with the gradual addition of HSO_4^- and $H_2PO_4^-$ (Figure 8 and Figures S28−S31 (Supporting Information)). The different optical signal responses obtained for F^-, CN^-, AcO^-, SO_4^{2-}, HSO_4^-, and $H_2PO_4^-$ are due to the differences in charge density, size, and basicity of the anions. Table 3 also summarizes all of the emission data derived equilibrium constants measured for the receptors toward different anions.

It may be noted that the values of the equilibrium constant (K) for the metalloreceptors with CN^-, F^-, AcO^-, SO_4^{2-}, and $H_2PO_4^-$ are grossly over 6 orders of magnitudes. In general, the values of K obtained by the spectrophotometric method compare reasonably well with the values obtained by the spectrofluorometric method. We have tried to correlate the values of K with a particular anion with different complexes. However, we are unable to reach a definite correlation. Moreover, considering the K values (Table 3) of a particular receptor, the general order of sensitivity is grossly the following: $CN^- > F^- > AcO^- \approx SO_4^{2-} > H_2PO_4^-$.

One of the most important parameters in anion sensing is the detection limit. For many practical purposes, it is important to sense anions at extremely low concentrations. The detection limits of complexes **1**−**5** were obtained according to the literature method.[15e,48,49] The absorption and luminescence spectral changes during the titration of the complexes (2.0×10^{-5} M) with anions (5.0×10^{-3} M) in acetonitrile/dichloromethane (1/9 v/v) solution have already been shown in Figure 7 and Figures S19−S31 (Supporting Information). The curves plotted for normalized absorbance or luminescence intensity vs log [anion] are shown in Figures S32−S41 (Supporting Information). Linear regression curves fitted to the intermediate values are also shown in Figures S32−S41 (Supporting Information). The point at which the line crosses the ordinate axis is taken as the detection limit of the anion. Thus, on the basis of the absorption and fluorescence titration measurements, detection limits of the metalloreceptors for F^-, CN^-, and AcO^- were determined (Figures S32−S41, Supporting Information) and the values are presented in Table S8 Supporting Information). It is of interest to note that the spectrophotometric and fluorometric detection limits of the receptors for the said anions lie in the range of $(4.26-8.36) \times 10^{-9}$ M. Thus, the metalloreceptors can be applied for detection of F^-, CN^-, and AcO^- at concentrations as low as 10^{-9} M, which might meet the requirements for biosensing.[48,49]

Luminescent transition-metal complexes continue to attract considerable interest as sensors because they have relatively long lifetimes in comparison to their purely organic counterparts and it is becoming clear that lifetime-based detection has significant advantages over intensity methods.[50,51] In this context, luminescence lifetimes of the receptors were measured in acetonitrile/dichloromethane (1/9 v/v) at room temperature as a function of increasing concentration of F^-, SO_4^{2-}, HSO_4^-, and $H_2PO_4^-$ ions, and the decay profiles are represented in Figure 9 and Figures S42−S44 (Supporting Information). In the absence of anions, all of the metalloreceptors exhibit a biexponential decay with their lifetimes shown in the inset of Figure 9 and Figures S42−S44 (Supporting Information). On incremental addition of both F^- and SO_4^{2-} ions, there is a gradual decrease of lifetime in general for both the first and second components and the decays again can be fitted with a sum of two exponentials (lifetimes are given in the inset of Figure 9 and Figure S42 (Supporting Information)). In contrast, when HSO_4^- or $H_2PO_4^-$ is added to the solutions of the receptors, somewhat different behaviors are observed. During the first two additions of the ions, the lifetimes of both the first and the second components of all the complexes increase in general. On further addition of these anions, the lifetimes of the first component decrease while those of the second component either remain invariant or slightly increase (Figures S43 and S44, Supporting Information). These data suggest that, on gradual addition of either F^- or SO_4^{2-} ions, deprotonation of the imidazole NH protons occurs and the lifetimes of the deprotonated species became shorter than those of the free receptors; the net result is the observed lifetime quenching shown in Figure 9 and Figure S42 (Supporting Information). On the other hand, with HSO_4^- and $H_2PO_4^-$, the data indicate that there are at least two distinct luminescent species. The species probably consist of the hydrogen-bonded adduct of the receptor with HSO_4^- or $H_2PO_4^-$, whose lifetime is longer, and the free receptor, whose lifetime is shorter, the sum of which results in the observed lifetime enhancement as shown in Figures S43 and S44 (Supporting Information). It may be mentioned that the intensity of the steady-state emission maximum also gradually increases with the addition of

dx.doi.org/10.1021/ic3022326 | Inorg. Chem. 2013, 52, 6820−6838

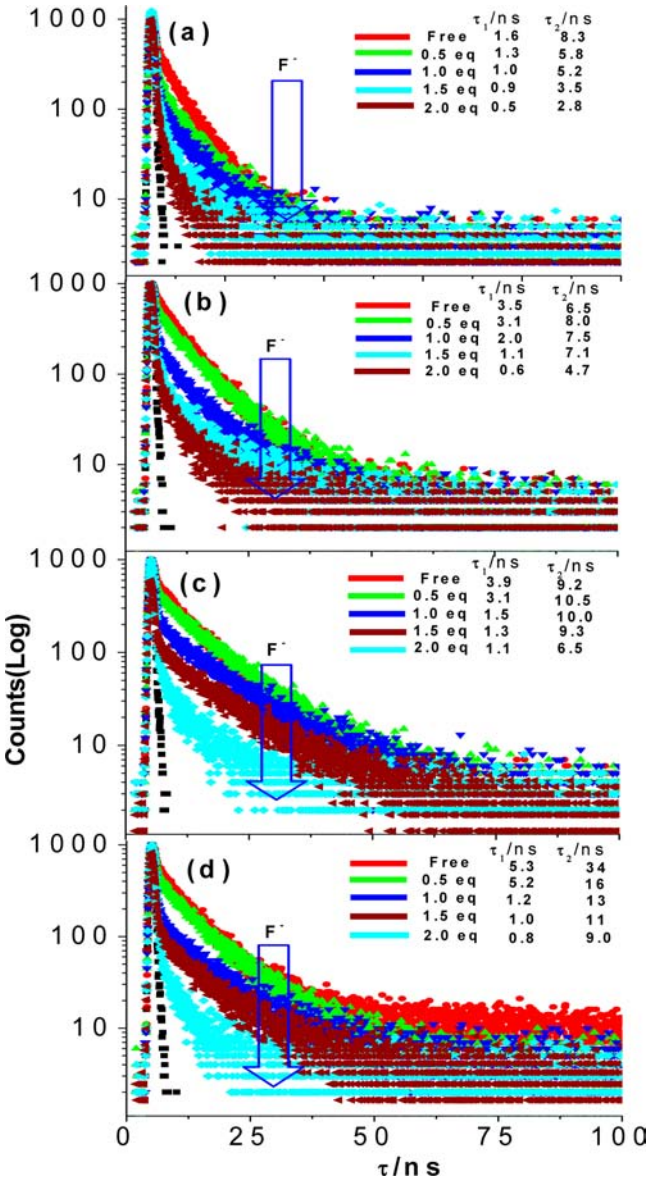

Figure 9. Changes in the time-resolved luminescence decays of **1** (a), **2** (b), **3** (c), and **5** (d) in acetonitrile/dichloromethane (1/9 v/v) solution (2.0×10^{-5} M) at room temperature upon the incremental addition of F^- ion (5.0×10^{-3} M). Insets show the lifetimes of the complexes.

both HSO_4^- and $H_2PO_4^-$ ions. It should be noted that several Ru(II) polypyridyl based metalloreceptors for $H_2PO_4^-$ have been previously reported and it was seen that both the emission intensity and lifetime of the receptors increase on addition of $H_2PO_4^-$.[52] It is suggested that, due to binding of $H_2PO_4^-$ ions with a luminescent receptor, the increase in emission intensity occurs because the bound anion serves to rigidify the receptor and thus inhibit vibrational and rotational relaxation modes of nonradiative decay. Luminescence enhancement in our case may be due to this rigidity effect of the metalloreceptor when it binds with HSO_4^- and $H_2PO_4^-$ through a hydrogen-bonding interaction.[18,20,52] Thus, the anion-induced lifetime modulation makes the complexes suitable lifetime-based sensors for selective anions.

To prove the interaction of metalloreceptors with various anions, ^{1}H NMR titrations were carried out with additions of increasing amounts of anions (F^-, CN^-, and $H_2PO_4^-$ ions) to DMSO-d_6 or CD_3CN solutions of the complexes. Typically a 5.0×10^{-3} M solution of **3** in DMSO-d_6 was titrated with F^- ion up to 2 equiv. Figure 10 shows that the two imidazole N−H protons of coordinated H_2pbbzim appeared as a singlet at 15.03 ppm in the ^{1}H NMR spectrum. The NH signal appeared in a profoundly downfield region due to strong hydrogen bonding with DMSO-d_6. Upon gradual addition of F^-, the signal due to the NH protons becomes broadened and finally vanished when almost 1 equiv of F^- was added. It is of interest to note that with the titration of the F^- ion the integrated proportion of the N−H signal at about 15.03 ppm decreased progressively with the chemical shift remaining almost stable, indicating a typical deprotonation of the N−H group.[53] Importantly, the chemical shifts of C−H protons of H_2pbbzim (H_{16}, H_{17}, H_{18}, H_{19}, H_{20}, and H_{21}) are also very sensitive upon addition of F^- ion. Figure 10 shows that the chemical shifts of the above protons get shifted progressively upfield on gradual addition of F^- ion to a solution of **3**. A similar behavior was also observed with CN^- ion. The ^{1}H NMR spectral changes of **3** that occurred with incremental addition of CN^- ions are shown in Figure S45 (Supporting Information) and the change of chemical shifts for the above benzimidazole protons as a function of the amount of CN^- added is shown in Figure S46 (Supporting Information). Clearly, F^- and CN^- ions act as proton abstractors and the shielding effect is a consequence of the increase in electron density of the imidazole moiety due to the deprotonation of the N−H protons and subsequent delocalization of the negative charge throughout the aromatic frame.[15,25]

In order to check the mode of interaction of the receptors with $H_2PO_4^-$ ion, an ^{1}H NMR titration experiment of **3** was also carried out in CD_3CN solution with incremental amounts of $H_2PO_4^-$ ion (Figure S47, Supporting Information). In CD_3CN, the signal due to N−H protons appeared at 12.80 ppm, indicating that the extent of hydrogen bonding of the NH proton with CD_3CN is less than that with DMSO-d_6. It is of interest to note that, during the initial addition of $H_2PO_4^-$ ion to the CD_3CN solution of **3**, the signal at 12.80 ppm due to NH protons becomes intensified and at the same time shifted considerably downfield. Further addition of $H_2PO_4^-$ ion leads to broadening and finally removal of the NH signal, followed by precipitation of the resulting complex. Thus, significant broadening and downfield shifts of the NH signals in the ^{1}H NMR spectra of **3** upon addition of $H_2PO_4^-$ indicate that the probable mode of interaction of the receptors with $H_2PO_4^-$ ion is through hydrogen bonding.[53] It should also be noted that the upfield shifts of C−H protons of H_2pbbzim (H_{16}, H_{17}, H_{18}, H_{19}, H_{20}, and H_{21}) moiety are much less in comparison to the shifts in the presence of F^- and CN^- ions in DMSO-d_6. Previously, we have noticed very minor changes in absorption spectral traces of the receptors (**1**−**5**) upon the addition of $H_2PO_4^-$, implying only a hydrogen-bonding interaction, which is again supported by the ^{1}H NMR titration experiment. On the other hand, a significant upfield shift of C−H proton signals of H_2pbbzim in conjunction with a profound red shift in the UV−visible absorption spectra of the metalloreceptors in the presence of F^- and CN^- indicates an increasing shielding effect on the benzimidazole protons and suggests neat proton transfer occurring from the imidazole N−H to the anions. Stepwise deprotonation of the two imidazole NH protons in the metalloreceptors was also confirmed by the titration in *n*-Bu_4NOH. The very similar UV−vis absorption titration isotherms upon the addition of F^-, CN^-, and OAc^- in

dx.doi.org/10.1021/ic3022326 | Inorg. Chem. 2013, 52, 6820−6838

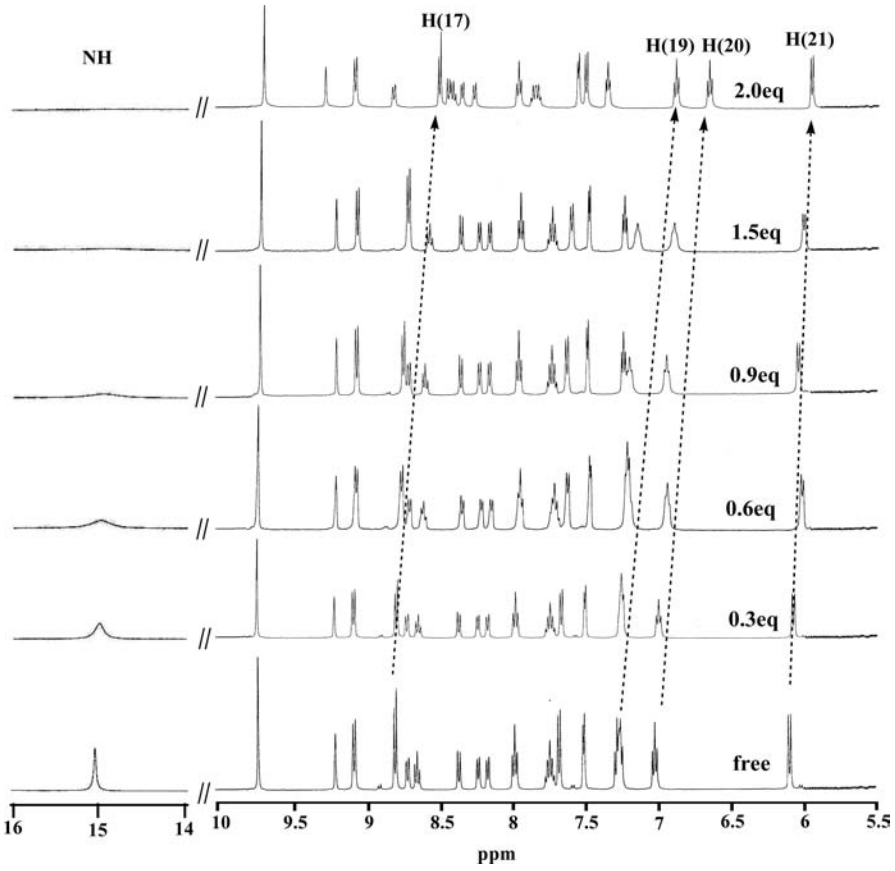

Figure 10. ^{1}H NMR titration of sensor **3** in DMSO-d_6 solution (5.0×10^{-3} M) upon addition of F^- ion (1.25×10^{-1} M, 0–2 equiv).

comparison with that of OH^- strongly suggest that the complexes undergo a stepwise proton transfer in the presence of F^-, CN^-, or OAc^-. The less basic $H_2PO_4^-$ and HSO_4^- ions show no ability to deprotonate the imidazole N–H protons and, thus, form only simple 1/1 hydrogen-bonded complexes upon the addition of 1 equiv of $H_2PO_4^-$ or HSO_4^- ion.[53]

^{1}H NMR spectra of **2** and **5** in the presence of 5 equiv of TBAF were also recorded (Figures S48 and S49, Supporting Information), and the chemical shift values are collected in Table S9 (Supporting Information). In all of the cases complete removal of the most downfield-shifted resonance due to the NH protons occurs along with an upfield shift of the aromatic proton of the H_2pbbzim moiety. As expected, the chemical shifts of the aromatic protons due to tpy-Ar ligands differ only to a small extent in the complexes.

The electrochemical anion recognition and sensing of the receptors as a function of different anions were carried out in CH_3CN solutions by using cyclic and square wave voltammetry. As shown in Figure 11, with incremental addition of AcO^- to the acetonitrile solution of **4**, the current height of the oxidation couple observed at 1.10 V gradually diminishes, and at its expense two new couples that appear at 0.48 and 0.94 V grow in current heights until the AcO^- ion concentration reaches 1 equiv. Beyond 1 equiv, the couples at both 1.10 and 0.94 V continued to decease in intensity and eventually were completely replaced by the 0.48 V couple. The electrochemical behavior observed with other anions such as F^-, CN^-, and SO_4^{2-} as the guest anions is almost identical with that of AcO^- for **4**. Moreover, the cyclic and square wave voltammograms of the other complexes follow the same trends with increasing concentrations of the anions (Figures S50 and S51, Supporting Information). It is evident that, on progressive addition of F^-, CN^-, and AcO^- ions to the acetonitrile solutions of the complexes (**1**–**5**), the oxidation potentials are substantially

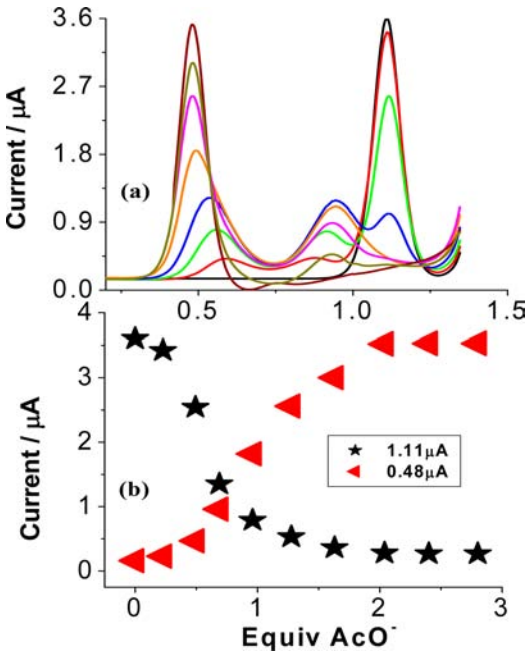

Figure 11. (a) SWVs of **4** obtained upon incremental addition of AcO^- ion (2.0×10^{-2} M) to its acetonitrile solution (2.5×10^{-4} M). (b) Changes in the current intensities as a function of the amount of AcO^- ion added.

dx.doi.org/10.1021/ic3022326 | Inorg. Chem. 2013, 52, 6820–6838

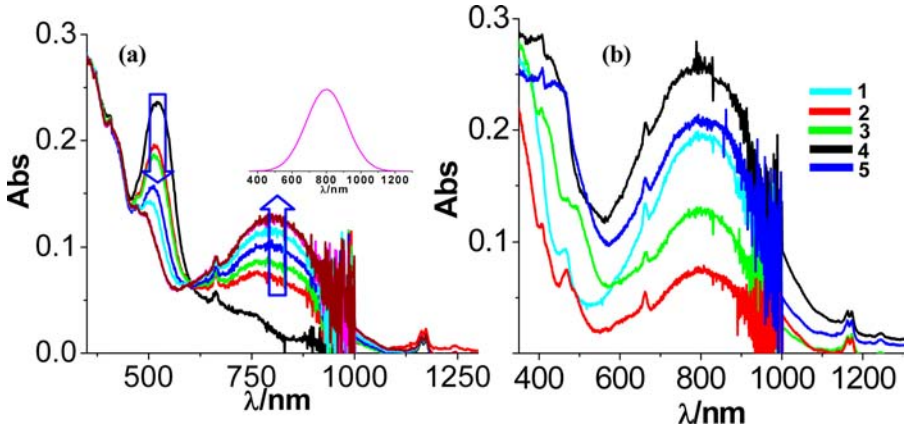

Figure 12. (a) Spectroelectrochemical changes during the oxidation of [(pbbzim)Ru(tpy-Naph] (**3a**). The inset shows the deconvoluted LMCT band. (b) Spectra obtained after complete oxidation of the deprotonated complexes.

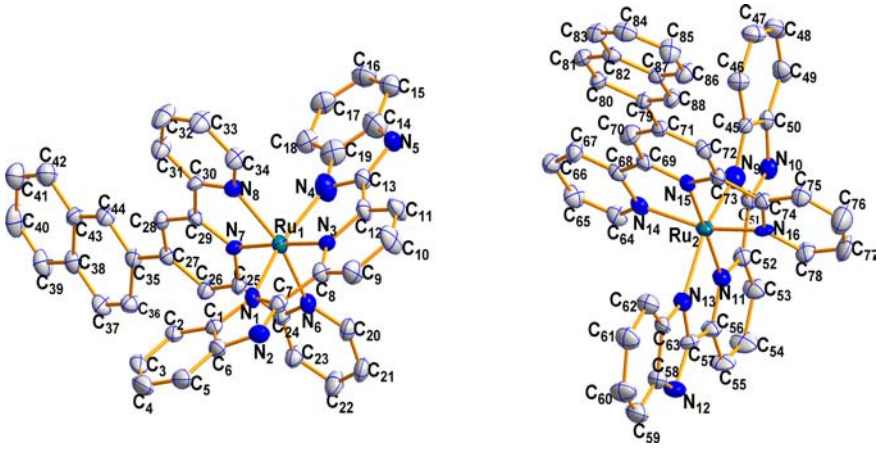

Figure 13. ORTEP[35] representation of the complex **3a** with 30% probability ellipsoids. The solvents of crystallization and the hydrogen atoms are omitted for clarity.

shifted to less positive potentials, in comparison to their corresponding protonated forms. Thus, in the presence of an excess of the anion, imidazole NH protons become successively deprotonated, thereby increasing the electron density on the metal center and causing a negative shift of the oxidation potential. The results nicely demonstrate that the complexes have the potential for the construction of suitable electrochemical sensors.

Spectroelectrochemical measurements were also carried out for the deprotonated complexes in acetonitrile, and the spectral changes that take place for the complexes are shown in Figure 12 and Figure S52 (Supporting Information). The overall changes in the spectral profiles of the complexes are basically similar, with distinct changes in their absorption spectral profiles and clear isosbestic points. Similar to the case for their protonated counterparts, during electrochemical oxidation, the metal to ligand charge transfer (MLCT) band of the compounds gradually disappears at the expense of the evolution of a ligand to metal charge transfer (tpy-Ar → Ru^{III} LMCT) band at considerably higher wavelengths. Moreover, the LMCT bands of the deprotonated complexes are substantially more red-shifted than those of their protonated forms.

X-ray Crystallographic Evidence for the Deprotonation of Imidazole NH Protons. To prove whether the observed changes in color and other optical and redox properties are caused by strong hydrogen bonding with the anions or by the deprotonation of the imidazole NH protons, single crystals were grown upon diffusing hexane into acetone/dichloromethane (1/1 v/v) solutions in presence of an excess of TBAF. The X-ray structural studies showed that the crystals of **3a** were of (**3**-$2H^+$) and that deprotonation of the two imidazole N−H protons occurred from the H_2pbbzim moiety. An ORTEP representation of the complex [(pbbzim)Ru(tpy-Naph)] (**3a**) is shown in Figure 13, and selected bond distances and angles are given in Table S1 (Supporting Information). The deprotonated complex also crystallized in a triclinic form with two crystallographically independent molecules in the unit cell. Similar to the structure of the corresponding protonated complex, the deprotonated form also displays the expected distorted-octahedral geometry, with both ligands coordinated in a tridentate meridional fashion to the Ru(II) center. It is of interest to note that the extent of the twist between the central pyridine ring and the naphthyl moiety becomes less and the value of the twist angle decreases from 23.47 to 6.43° on deprotonation. Again, similar to the case for its protonated analogue, intermolecular aromatic $\pi-\pi$ and CH$-\pi$ interactions also occur in the deprotonated complex and the metrical parameters involved therein can be seen in Figures S53−S55 (Supporting Information).

Ground- and Excited-State pK_a Values of the Complexes. Inasmuch as the imidazole NH protons of H_2pbbzim in the complexes can be subjected to deprotonation,

dx.doi.org/10.1021/ic3022326 | *Inorg. Chem.* 2013, 52, 6820−6838

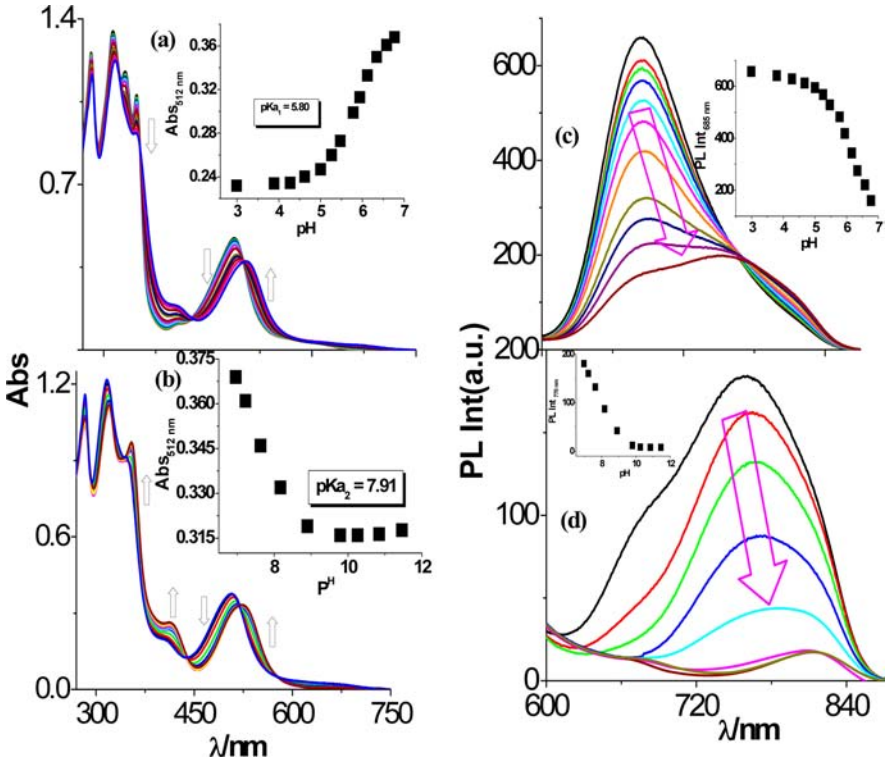

Figure 14. Changes in the absorption (a and b) and photoluminescence spectra (c and d) of **3** with variation of pH in acetonitrile/water (3/2 v/v). The insets show the change in absorbance (a and b) and luminescence (c and d) with pH.

we have been interested in determining the pK_a values for the complexes and compare them with their anion binding/equilibrium constants. In order to do so, the influence of pH on the absorption spectra of the complexes has also been studied quantitatively by performing spectrophotometric titrations of the complexes in CH_3CN/H_2O (3/2 v/v) solutions over the pH range 2.5−12. The spectrum of **3**, typical of all (Figure 14), remains unchanged in the low pH range 2.5−3.5. However, as the pH is increased from 3.5 to 7.0, the absorption maximum at 490 nm is progressively red-shifted to 506 nm with isosbestic points arising at 500, 428, and 352 nm; on further increase of the pH, the bands are additionally red-shifted through a new set of isosbestic points at 518 and 440 nm until the maximum at 526 nm appears at pH 9.5, beyond which no further change occurs. The appearance of successive isosbestic points with an increase of pH provides a good indication of the involvement of two successive deprotonation equilibria. Taken together, the acid−base equilibria of the complexes can be described as

$$[(\text{tpy-Ar})\text{Ru}^{\text{II}}(\text{H}_2\text{pbbzim})]^{2+} \underset{\text{H}^+}{\overset{K_{a1}}{\rightleftharpoons}} [(\text{tpy-Ar})\text{Ru}^{\text{II}}(\text{Hpbbzim})]^{+} \underset{\text{H}^+}{\overset{K_{a2}}{\rightleftharpoons}} [(\text{tpy-Ar})\text{Ru}^{\text{II}}(\text{pbbzim})]$$

The pH vs absorbance curves for the remaining four complexes (**1**, **2**, **4**, and **5**) also show patterns similar to that of **3**, except for the intensities and the positions of the MLCT band maxima (Figures S56−S59, Supporting Information). The individual pK_a values (pK_{a1} and pK_{a2}) of the complexes have been evaluated using eq 2 from the two segments of the spectrophotometric titration data (Table S10, Supporting Information). Table S10 shows that both the pK_{a1} and pK_{a2} values of the complexes vary in a narrow range (5.5−5.8 for pK_{a1} and 7.7−8.1 for pK_{a2}). Thus, although the positions and the intensities of the MLCT bands are slightly controlled by the $Ru(tpy\text{-}Ar)^{2+}$ chromophores, the pK_a values of the complexes are far less affected by the variation of the aromatic rings. The similarity of the absorption spectra of the complexes in acetonitrile/dichloromethane (1/9 v/v) in the presence of selective anions (F^-, AcO^-, CN^-, and SO_4^{2-}) to the spectra with varying pH in 3/2 v/v acetonitrile/water mixtures suggests that the change in color and the spectral properties are a consequence of successive deprotonation of NH fragments of the coordinated H_2pbbzim. In the previous section, equilibrium/binding constants (K) for the receptor−anion interaction have been evaluated by using eq 1 and the values were summarized in Table 3. It may be noted that the values of K for the receptors with F^-, AcO^-, and CN^- ions span grossly 6 orders of magnitudes. Comparable values of the proton dissociation constants (K_a) have also been determined by performing spectrophotometric titrations of the complexes in CH_3CN/H_2O (3/2 v/v) solutions over the pH range 2.5−12.

The influence of pH on the emission spectra of the complexes has also been studied by performing luminescence titrations in CH_3CN/H_2O (3/2 v/v) solutions over the pH range 2.5−12. The spectrum of **3**, typical of all, is shown in Figure 14c,d. As the pH is increased from 3.5 to 7.0, the emission maximum at 685 nm is significantly quenched with a small red shift; on further increase of the pH, the band is red-shifted gradually to 815 nm with almost complete quenching of emission intensity at pH 9.5, beyond which no further change occurs (Figure 14d). Figures S56−S59 (Supporting Information) show the pH dependence of luminescence spectra of complexes **1**, **2**, **4**, and **5**. The dependence of luminescence lifetimes of **3** as a function of pH is also represented in Figure 15. The lifetimes remained nearly constant (17.0 ns) up to pH

dx.doi.org/10.1021/ic3022326 | Inorg. Chem. 2013, 52, 6820−6838

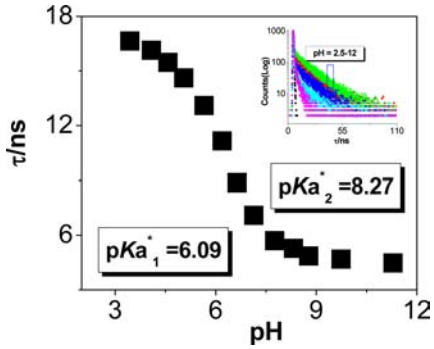

Figure 15. Change of the excited-state lifetimes of **3** with variation of pH in acetonitrile/water (3/2 v/v). The inset shows the decay profiles of **3** as a function of pH. Excited-state pK_a* values are also given in the figure.

3.5. Then the lifetime decreases gradually from 17.0 to 9.0 ns until the pH reaches to 6.5. Again, between pH 7.0 and 9.5, the lifetimes decrease steadily from 8.9 to 5.0 ns, beyond which no further change occurs. Similar two-step decreases of lifetimes for **1**, **2**, **4**, and **5** with increasing pH are shown in Figures S60–S63 (Supporting Information). It should be noted that the emission lifetime of **3** measured in 3/2 v/v acetonitrile/water buffer solution at pH 2.5 is 17.0 ns, in comparison to 15.0 ns in pure dichloromethane. The spectrophotometric data were used previously to determine the ground-state pK_a values of the complexes, and the luminescence data can be utilized to determine the excited-state acid dissociation constants (pK_a*). Since the pH ranges coincide with that observed for the ground-state deprotonation of the coordinated imidazole NH protons in the complexes in the UV–vis titration, the above emission spectral changes are thus assigned to the excited-state deprotonation of the same proton, as in the ground state. Excited-state pK_a values could be obtained from luminescence intensity and lifetime data following the methods developed by Ireland and Wyatt.[54] Taking into account that the coordinated H_2pbbzim ligand has two titratable protons which are assumed to dissociate in two measurable steps,[55] the pK_a* values for each step can be determined by using eq 3, where pH is the

$$pK_a^* = \mathrm{pH} + \log \tau_{acid}/\tau_{base} \quad (3)$$

inflection point of the curve of emission intensity as a function of pH and τ_{acid} and τ_{base} correspond to the lifetimes of the protonated and deprotonated states, respectively. The lifetime values are experimentally obtained at pH levels well above and well below the midpoint, where τ is relatively invariant with pH. Thus, taking the inflection point pH value of 5.82 (Figure 15) and the lifetimes of 17 and 9 ns for the protonated and monodeprotonated states of **3**, respectively, a pK_{a1}* value of 6.09 is calculated for the first deprotonation step. On the other hand, a pK_{a2}* value of 8.27 is obtained for the second deprotonation process by using the obtained inflection point pH value of 8.02 and the lifetimes of 8.9 and 5 ns for the monodeprotonated and doubly deprotonated states of **3**. The excited-state pK_a values of the other complexes calculated in the same way are presented in Table S10 (Supporting Information). The results indicate that the first and second excited-state pK_a values (pK_{a1}* and pK_{a2}*) are both higher than the ground-state pK_a values in all of the complexes. A comparison of ground-state and excited -state acid dissociation constants is useful, because the relative change in the pK_a provides qualitative information on the localization of charge in MLCT states.[55] The excited-state pK_a* values are higher than the ground state values for the same process, implying that the MLCT state is localized on the H_2pbbzim moiety (the excited state has increased negative charge and is therefore less acidic).[56–58]

Nature of Receptor–Anion Interactions. The observations made above from absorption, emission, ^{1}H NMR, and electrochemical measurements unequivocally suggest that F^-, AcO^-, CN^-, and SO_4^{2-} interact strongly with the metalloreceptors, although such interactions are either very weak or absent for other halides (Cl^-, Br^-, I^-) and oxyanions (NO_3^-, and ClO_4^-). The close similarity of the spectral patterns (both absorption and emission) of the receptors in CH_3CN/H_2O (3/2 v/v) as a function of pH with those in the presence of selective anions suggests that H_2pbbzim in the complexes successively deprotonates to Hpbbzim$^-$ and finally to pbbzim^{2-} in the presence of excess anion. It is observed that the mode of interaction of HSO_4^- and $H_2PO_4^-$ ions with the metallorecptors is somewhat different. It would appear at first that the role of the anions (F^-, AcO^-, CN^-, and SO_4^{2-}) is simply to abstract the N–H protons. However, there is growing evidence to suggest that the picture could be far from simple.[17–25,59,60] It appears that hydrogen bonding, supramolecular interactions of the second coordination sphere, and proton transfer reactions probably come into play. In the present case, we envisage that the imidazole N–H protons of the receptors interact with selective anions X^- (F^-, AcO^-, CN^-, and SO_4^{2-}) to form incipient N–H- - -X^- hydrogen bonds and the presence of excess X^- induces further stretching of the N–H bond, which eventually splits through a proton transfer reaction. The evidence suggests that the second step is probably not operative with HSO_4^- and $H_2PO_4^-$, as these ions are acidic in comparison to other ions such as F^-, AcO^-, CN^-, and SO_4^{2-}. Finally, we note that although the receptors **1**–**5** exhibit strong response toward sensing F^-, CN^-, AcO^-, and SO_4^{2-} and to some extent $H_2PO_4^-$ and HSO_4^-, they lack selectivity to differentiate these anions explicitly.

CONCLUSION

In conclusion, we have developed a new series of heteroleptic bis-tridentate ruthenium(II) complexes by using the tridentate ligand 2,6-bis(benzimidazol-2-yl)pyridine (H_2pbbzim) and different 4′-aryl (phenyl, 2-naphthyl, 9-anthryl, and 1-pyrenyl) substituted terpyridine derivatives wherein a potentially luminescent polyaromatic moiety is directly linked to the 4′-position of a terpyridine unit via a C–C single bond. The most important outcome of this study is that the complexes are luminescent at room temperature in fluid solutions and their room temperature lifetimes lie in the range of 5.5–62 ns, depending upon the polyaromatic substituent as well as solvent polarity. The sub-nanosecond excited-state lifetime of normal tpy complexes is widely accepted as being due to the small energy gap between the emitting ^{3}MLCT state and the deactivating ^{3}MC level. Another point of interest is that, owing to the presence of imidazole NH protons, which became appreciably acidic due to metal coordination, the complexes can be utilized for multichannel recognition of selective ions such as F^- and AcO^- ions in solution. The anion -sensing properties of the complexes have been studied by absorption, steady-state and time-resolved emission, and ^{1}H NMR spectroscopic and cyclic voltammetric techniques. The observations made from

dx.doi.org/10.1021/ic3022326 | Inorg. Chem. 2013, 52, 6820–6838

the above physicochemical measurements and X-ray crystallographic studies unequivocally suggest that metal-coordinated H_2pbbzim in **1**−**5** becomes successively deprotonated to Hpbbzim$^-$ and finally to pbbzim^{2-} in the presence of excess anion (F^-, AcO^-, CN^-, and SO_4^{2-}). Less basic anions such as $H_2PO_4^-$ and HSO_4^-, on the other hand, show no ability to deprotonate the imidazole N−H protons and, thus, form only hydrogen-bonded complexes. Further, the sequential changes that occur in the absorption spectra of the complex with the stepwise oxidation of the metal centers have been followed by spectroelectrochemical measurements. With stepwise oxidation of the Ru(II) centers replacement of MLCT bands by LMCT bands occurs in both the protonated and deprotonated forms of the complexes.

■ ASSOCIATED CONTENT

Ⓢ Supporting Information

CIF files, tables, and figures giving crystallographic data for **3**, **3a**, and **5**, including bond distances (Å) and angles (deg), $\pi-\pi$, CH$-\pi$ and O−CH interactions, ^{1}H NMR data, electrochemical data, absorption spectral data on spectroelectrochemical oxidation, detection limits, ^{1}H NMR data for **1**−**3** and **5** in the presence of 5 equiv of F^-, ground- and excited-state p*K*s, ESI-MS (positive), capped-stick projections of **3** and **5** showing $\pi-\pi$, CH$-\pi$ and anion−CH interactions, ^{1}H NMR spectra of **2**−**5** in DMSO-d_6, ^{1}H−^{1}H COSY spectra of **3** and **5**, time-resolved luminescence decay, CVs, spectroelectrochemical changes during oxidation, color changes of **2** and **4** with anions, UV−vis and luminescence spectral changes as a function of of different anions, detection limits, time-resolved luminescence decay, ^{1}H NMR titration, CVs, and SWVs of **2** and **5** as a function of AcO^- ions, spectroelectrochemical changes during oxidation of the deprotonated complexes, capped-stick projections of **3a** showing $\pi-\pi$, CH$-\pi$, and anion−CH interactions, absorption, photoluminescence and lifetime changes with pH, and ground- and excited-state pK_as. This material is available free of charge via the Internet at http://pubs.acs.org.

■ AUTHOR INFORMATION

Corresponding Author

*E-mail for S.B.: sbaitalik@hotmail.com.

Notes

The authors declare no competing financial interest.

■ ACKNOWLEDGMENTS

Financial assistance received from the Department of Science and Technology, New Delhi (Grant No. SR/S1/IC-33/2010), is gratefully acknowledged. Thanks are due to the DST for providing the single-crystal X-ray difractometer in FIST and time-resolved nanosecond spectrofluorimeter in the PURSE program at the Department of Chemistry of Jadavpur University. D.M. and S.D. thank the CSIR and S.M. thanks the UGC for their fellowships.

■ REFERENCES

(1) (a) Juris, A.; Balzani, V.; Barigelletti, F.; Campagna, S.; Belser, P.; von Zelewsky, A. *Coord. Chem. Rev.* **1988**, *84*, 85. (b) Balzani, V.; Juris, A.; Venturi, M.; Campagna, S.; Serroni, S. *Chem. Rev.* **1996**, *96*, 759. (c) Sauvage, J.-P.; Collin, J. P.; Chambron, J. C.; Guillerez, S.; Coudret, C.; Balzani, V.; Barigelletti, F.; De Cola, L.; Flamigni, L. *Chem. Rev.* **1994**, *94*, 993. (d) Balzani, V. *Photochem. Photobiol. Sci.* **2003**, *2*, 459.

(2) (a) Meyer, T. J. *Pure Appl. Chem.* **1986**, *58*, 1193. (b) Meyer, T. J. *Acc. Chem. Res.* **1989**, *22*, 163.

(3) (a) Baranoff, E.; Collin, J. P.; Flamigni, L.; Sauvage, J.-P. *Chem. Soc. Rev.* **2004**, *33*, 147. (b) Beyler, A.; Belser, P. *Coord. Chem. Rev.* **2002**, *230*, 28.

(4) (a) Balzani, V.; Credi, A.; Venturi, M. *Molecular Devices and Machines*; Wiley-VCH: Weinheim, Germany, 2003. (b) Scandola, F.; Chiorboli, C.; Indelli, M. T.; Rampi, M. A. In *Electron Transfer in Chemistry*; Balzani, V.;, Ed.; Wiley-VCH: Weinheim, Germany, 2001; Vol. 3, p 337. (c) Sun, L.; Hammarström, L.; Akermark, B.; Styring, S. *Chem. Soc. Rev.* **2001**, *30*, 36. (d) Baitalik, S.; Wang, X.; Schmehl, R. H. *J. Am. Chem. Soc.* **2004**, *126*, 16304. (e) Wang, X.; Guerzo, A.; Baitalik, S.; Simon, G.; Shaw, G. B.; Chen, L. X.; Schmehl, R. *Photosynth. Res.* **2006**, *87*, 83. (f) Liu, Y.; DeNicola, A.; Ziessel, R.; Schanze, K. S. *J. Phys. Chem. A* **2003**, *107*, 3476. (g) Alstrum-Acevedo, J. H.; Brennaman, M. K.; Meyer, T. J. *Inorg. Chem.* **2005**, *44*, 6802. (h) Browne, W. R.; O'Boyle, N. M.; McGarvey, J. J.; Vos, J. G. *Chem. Soc. Rev.* **2005**, *34*, 641. (i) Balzani, V.; Clemente-Léon, M.; Credi, A.; Ferrer, B.; Venturi, M.; Flood, A. H.; Stoddart, J. F. *Proc. Natl. Acad. Sci. U.S.A.* **2006**, *103*, 1178. (j) Kuang, D.; Ito, S.; Wenger, B.; Klein, C.; Moser, J.-E.; Humphry-Baker, R.; Zakeeruddin, S. M.; Gratzel, M. *J. Am. Chem. Soc.* **2006**, *128*, 4146 and references therein.

(5) (a) Knof, U.; von Zelewsky, A. *Angew. Chem., Int. Ed.* **1999**, *38*, 302. (b) Bodige, S.; Kim, M. −J.; MacDonnell, F. M. *Coord. Chem. Rev.* **1999**, *185*−*186*, 535. (c) Keene, F. R. *Chem. Soc. Rev.* **1998**, *27*, 185.

(6) (a) Constable, E. C. *Chem. Soc. Rev.* **2007**, *36*, 246. (b) Hofmeier, H.; Schubert, U. S. *Chem. Soc. Rev.* **2004**, *33*, 373. (c) Medlycott, E. A.; Hanan, G. S. *Coord. Chem. Rev.* **2006**, *250*, 1763. (d) Medlycott, E. A.; Hanan, G. S. *Chem. Soc. Rev.* **2005**, *34*, 133. (e) Wang, X.-Y.; Del Guerzo, A.; Schmehl, R. H. *J. Photochem. Photobiol. C* **2004**, *5*, 55.

(7) Winkler, J. R.; Netzel, T.; Creutz, C.; Sutin, N. *J. Am. Chem. Soc.* **1987**, *109*, 2381.

(8) (a) Maestri, M.; Armaroli, N.; Balzani, V.; Constable, E. C.; Thompson, A. M. W. C. *Inorg. Chem.* **1995**, *34*, 2759. (b) Wang, J.; Fang, Y. Q.; Hanan, G. S.; Loiseau, F.; Campagna, S. *Inorg. Chem.* **2005**, *44*, 5.

(9) (a) Fang, Y. Q.; Taylor, N. J.; Hanan, G. S.; Loiseau, F.; Passalacqua, R.; Campagna, S.; Nierengarten, H.; Van Dorsselaer, A. *J. Am. Chem. Soc.* **2002**, *124*, 7912. (b) Passalacqua, R.; Loiseau, F.; Campagna, S.; Fang, Y. Q.; Hanan, G. S. *Angew. Chem., Int. Ed.* **2003**, *42*, 1608. (c) Polson, M. I. J.; Loiseau, F.; Campagna, S.; Hanan, G. S. *Chem. Commun.* **2006**, 1301. (d) Fang, Y. Q.; Taylor, N. J.; Laverdiere, F.; Hanan, G. S.; Loiseau, F.; Nastasi, F.; Campagna, S.; Nierengarten, H.; Leize-Wagner, E.; Van Dorsselaer, A. *Inorg. Chem.* **2007**, *46*, 2854.

(10) (a) Benniston, A. C.; Grosshenny, V.; Harriman, A.; Ziessel, R. *Angew. Chem., Int. Ed.* **1994**, *33*, 1884. (b) Hissler, M.; El-ghayoury, A.; Harriman, A.; Ziessel, R. *Angew. Chem., Int. Ed.* **1998**, *37*, 1717. (c) Encinas, S.; Flamigni, L.; Barigelletti, F.; Constable, E. C.; Housecroft, C. E.; Schofield, E. R.; Figgemeier, E.; Fenske, D.; Neuburger, M.; Vos, J. G.; Zehnder, M. *Chem. Eur. J.* **2002**, *8*, 137. (d) Benniston, A. C.; Harriman, A.; Li, P.; Sams, C. A. *J. Am. Chem. Soc.* **2005**, *127*, 2553. (e) Wang, X-y.; Del Guerzo, A.; Tunuguntla, H.; Schmehl, R. H. *Res. Chem. Intermed.* **2007**, *33*, 63.

(11) (a) Duati, M.; Fanni, S.; Vos, J. G. *Inorg. Chem. Commun.* **2000**, *3*, 68. (b) Duati, M.; Tasca, S.; Lynch, F. C.; Bohlen, H.; Vos, J. G.; Stagni, S.; Ward, M. D. *Inorg. Chem.* **2003**, *42*, 8377.

(12) (a) Constable, E. C.; Dunne, S. J.; Rees, D. G. F.; Schmitt, C. X. *Chem. Commun.* **1996**, 1169. (b) Indelli, M. T.; Bignozzi, C. A.; Scandola, F.; Collin, J.-P. *Inorg. Chem.* **1998**, *37*, 6084.

(13) (a) Beley, M.; Collin, J.-P.; Louis, R.; Metz, B.; Sauvage, J.-P. *J. Am. Chem. Soc.* **1991**, *113*, 8521. (b) Wilkinson, A. J.; Puschmann, H.; Howard, J. A. K.; Foster, C. E.; Williams, J. A. G. *Inorg. Chem.* **2006**, *45*, 8685. (c) Wadman, S. H.; Lutz, M.; Tooke, D. M.; Spek, A. L.; Hartl, F.; Havenith, R.W. A.; van Klink, G. P. M.; van Koten, G. *Inorg. Chem.* **2009**, *48*, 1887.

(14) (a) Abrahamsson, M.; Jäger, M.; Österman, T.; Eriksson, L.; Persson, P.; Becker, H. C.; Johansson, O.; Hammarström, L. *J. Am. Chem. Soc.* **2006**, *128*, 12616. (b) Abrahamsson, M.; Lundqvist, M. J.; Wolpher, H.; Johansson, O.; Eriksson, L.; Bergquist, J.; Rasmussen, T.;

Becker, H.-C.; Hammarström, L.; Norrby, P.-O.; Åkermark, B.; Persson, P. *Inorg. Chem.* **2008**, *47*, 3540. (c) Abrahamsson, M.; Jäger, M.; Kumar, R. J.; Österman, T.; Persson, P.; Becker, H. C.; Johansson, O.; Hammarström, L. *J. Am. Chem. Soc.* **2008**, *130*, 15533.
(15) (a) Bhaumik, C.; Das, S.; Saha, D.; Dutta, S.; Baitalik, S. *Inorg. Chem.* **2010**, *49*, 5049. (b) Bhaumik, C.; Saha, D.; Das, S.; Baitalik, S. *Inorg. Chem.* **2011**, *50*, 12586. (c) Bhaumik, C.; Das, S.; Maity, D.; Baitalik, S. *Dalton Trans.* **2012**, *41*, 2427. (d) Bhaumik, C.; Das, S.; Maity, D.; Baitalik, S. *Dalton Trans.* **2011**, *40*, 11795. (e) Bhaumik, C.; Das, S.; Maity, D.; Baitalik, S. *RSC Adv.* **2012**, *2*, 2581.
(16) (a) Aoyama, Y.; Endo, K.; Anzai, T.; Yamaguchi, Y.; Sawaki, T.; Kobayashi, K.; Kanehisa, N.; Hashimoto, H.; Kai, Y.; Masuda, H. *J. Am. Chem. Soc.* **1996**, *118*, 5562. (b) Gulyani, A.; Gopalan, R. S.; Kulkarni, G. U.; Bhattacharya, S. *J. Mol. Struct.* **2002**, *616*, 103.
(17) Sessler, J. L.; Gale, P. A.; Cho, W. S. *Anion Receptor Chemistry*; Royal Society of Chemistry: Cambridge, U.K., 2006.
(18) Hargrove, A. E.; Nieto, S.; Zhang, T.; Sessler, J. L.; Anslyn, E. V. *Chem. Rev.* **2011**, *111*, 6603.
(19) (a) Beer, P. D.; Bayly, S. R. *Top. Curr. Chem.* **2005**, *255*, 125. (b) Caltagirone, C.; Gale, P. A. *Chem. Soc. Rev.* **2009**, *38*, 520. (c) Sessler, J. L.; Davis, J. M. *Acc. Chem. Res.* **2001**, *34*, 989. (d) Quang, D. T.; Kim, J. S. *Chem. Rev.* **2007**, *107*, 3780. (e) Mutihac, L.; Lee, J. H.; Kim, J. S.; Vicens, J. *Chem. Soc. Rev.* **2011**, *40*, 2777.
(20) Martínez-Máñez, R.; Sancenón, F. *Chem. Rev.* **2003**, *103*, 4419.
(21) Steed, J. W. *Chem. Soc. Rev.* **2009**, *38*, 506.
(22) (a) dos Santos, C. M. G.; Harte, A. J.; Quinn, S. T.; Gunnalaugsson, T. *Coord. Chem. Rev.* **2008**, *252*, 2512. (b) Gunnalaugsson, T.; Glynn, M.; Tocci, (nee Hussey), G. M.; Kruger, P. E.; Pfeffer, F. M. *Coord. Chem. Rev.* **2006**, *250*, 3094.
(23) (a) Peŕez, J.; Riera, L. *Chem. Commun.* **2008**, 533. (b) Peŕez, J.; Riera, L. *Chem. Soc. Rev.* **2008**, *37*, 2658.
(24) (a) Rice, C. R. *Coord. Chem. Rev.* **2006**, *250*, 3190. (b) Kumar, A.; Sun, S.-S.; Lees, A. J. *Coord. Chem. Rev.* **2008**, *252*, 922. (c) Amendola, V.; Gómez, E. D.; Fabbrizzi, L.; Licchelli, M. *Acc. Chem. Res.* **2006**, *39*, 343. (d) Suksai, C.; Tuntulani, T. *Top. Curr. Chem.* **2005**, *255*, 163. (e) Amendola, V.; Fabbrizzi, L. *Chem. Commun.* **2008**, 513.
(25) (a) Saha, D.; Das, S.; Maity, D.; Dutta, S.; Baitalik, S. *Inorg. Chem.* **2011**, *50*, 46. (b) Saha, D.; Das, S.; Bhaumik, C.; Dutta, S.; Baitalik, S. *Inorg. Chem.* **2010**, *49*, 2334. (c) Das, S.; Saha, D.; Bhaumik, C.; Dutta, S.; Baitalik, S. *Dalton Trans.* **2010**, *39*, 4162. (d) Saha, D.; Das, S.; Mardanya, S.; Baitalik, S. *Dalton Trans.* **2012**, *41*, 8886.
(26) (a) Yam, V. W. W. *Acc. Chem. Res.* **2002**, *35*, 555. (b) Wong, K. M. C.; Tang, W. S.; Lu, X. X.; Zhu, N.; Yam, V. W. W. *Inorg. Chem.* **2005**, *44*, 1492. (c) Yam, V. W. W.; Tang, R. P. L.; Wong, K. M. C.; Lu, X. X.; Cheung, K. K.; Zhu, N. *Chem.- Eur. J.* **2002**, *8*, 4066. (d) Yam, V. W. W.; Wong, K. M. C.; Zhu, N. *Angew. Chem., Int. Ed.* **2003**, *42*, 1400.
(27) (a) Anzebacher, P.; Tyson, D. S.; Jurslkova, K.; Castellano, F. N. *J. Am. Chem. Soc.* **2002**, *124*, 6232. (b) Mizuno, T.; Wei, W.-H.; Eller, L. R.; Sessler, J. L. *J. Am. Chem. Soc.* **2002**, *124*, 1134. (c) Beer, P. D.; Szemes, F.; Balzani, V.; Salà, C. M.; Drew, M. G. B.; Dent, S. W.; Maestri, M. *J. Am. Chem. Soc.* **1997**, *119*, 11864. (d) Cui, Y.; Mo, H.-J.; Chen, J.-C.; Niu, Y.-L.; Zhong, Y.-R.; Zheng, K.-C.; Ye, B.-H. *Inorg. Chem.* **2007**, *46*, 6427. (e) Lin, Z.-H.; Zhao, Y.-G.; Duan, C.-Y.; Zhang, B.-G.; Bai, Z.-P. *Dalton Trans.* **2006**, 3678. (f) Ion, L.; Morales, D.; Perez, J.; Riera, L.; Riera, V.; Kowenicki, R. A.; McPartlin, M. *Chem. Commun.* **2006**, 91. (g) Zapata, F.; Caballero, A.; Espinosa, A.; Tárraga, A.; Molina, P. *J. Org. Chem.* **2008**, *73*, 4034. (h) Derossi, S.; Adams, H.; Ward, M. D. *Dalton Trans.* **2007**, 33. (i) Lin, T.-P.; Chen, C.-Y.; Wen, Y.-S.; Sun, S.-S. *Inorg. Chem.* **2007**, *46*, 9201.
(28) Krohnke, F. *Synthesis* **1976**, 1.
(29) Schneider, H.-J.; Yatsimirsky, A. *Principles and Methods in Supramolecular Chemistry*; Wiley: Chichester, England, 2000; p 142.
(30) Perrin, D. D.; Dempsey, B. *Buffers for pH and Metal Ion Control*; Chapman and Hall: London, 1974.
(31) *SAINT (version 6.02)* and *SADABS (version 2.03)*; Bruker AXS Inc., Madison, WI, 2002.
(32) Sheldrick, G. M. *SHELXL-97, Program for the Refinement of Crystal Structures*; University of Göttingen, Göttingen, Germany, 1997.
(33) *SHELXTL (version 6.10)*; Bruker AXS Inc., Madison, WI, 2002.
(34) PLATON: Spek, A. L. *J. Appl. Crystallogr.* **2003**, *36*, 7-13.
(35) ORTEP-32 for Windows: Farrugia, L. J. *J. Appl. Crystallogr.* **1997**, *30*, 565.
(36) (a) Constable, E. C.; Lewis, J.; Liptrot, M. C.; Raithby, P. R. *Inorg. Chim. Acta* **1990**, *178*, 47. (b) Albano, G.; Balzani, V.; Constable, E. C.; Maestri, M.; Smith, D. R. *Inorg. Chim. Acta* **1998**, *277*, 225.
(37) Alcock, N. W.; Barker, P. R.; Haider, J. M.; Hannon, M. J.; Painting, C. L.; Pikramenou, Z.; Plummer, E. A.; Rissanen, K.; Saarenketo, P. *Dalton Trans.* **2000**, 1447.
(38) (a) Coe, B. J.; Thompson, D. W.; Culbertson, C. T.; Schoonover, J. R.; Meyer, T. J. *Inorg. Chem.* **1995**, *34*, 3385. (b) Kober, E. M.; Meyer, T. J. *Inorg. Chem.* **1982**, *21*, 3967.
(39) (a) Xiaoming, X.; Haga, M.; Inoue, T. M.; Ru, Y.; Addison, A. W.; Kano, K. *J. Chem. Soc., Dalton Trans.* **1993**, 2477. (b) Haga, M.; Takasugi, T.; Tomie, A.; Ishizuya, M.; Yamada, T.; Hossain, M. D.; Inoue, M. *Dalton Trans.* **2003**, 2069.
(40) (a) Liu, Y.; Hammitt, R.; Lutterman, D. A.; Thummel, R. P.; Turro, C. *Inorg. Chem.* **2007**, *46*, 6011. (b) Liu, Y.; Hammitt, R.; Lutterman, D. A.; Joyce, L. E.; Thummel, R. P.; Turro, C. *Inorg. Chem.* **2009**, *48*, 375.
(41) Hecker, C. R.; Gushurst, A. K. I.; McMillin, D. R. *Inorg. Chem.* **1991**, *30*, 538.
(42) Strouse, G. F.; Schoonover, J. R.; Duesing, R.; Boyde, S.; Jones, W. E., Jr.; Meyer, T. J. *Inorg. Chem.* **1995**, *34*, 473.
(43) Wang, J.; Hanan, G. S.; Loiseau, F.; Campagna, S. *Chem. Commun.* **2004**, 2068.
(44) (a) Vogler, L. M.; Brewer, K. J. *Inorg. Chem.* **1996**, *35*, 818. (b) Arana, C. R.; Abruña, H. D. *Inorg. Chem.* **1993**, *32*, 194.
(45) (a) Balzani, V.; Sabbatini, N.; Scandola, F. *Chem. Rev.* **1986**, *86*, 319. (b) Rampi, M. A.; Indelli, M. T.; Scandola, F.; Pina, F.; Parola, A. J. *Inorg. Chem.* **1996**, *35*, 3355.
(46) In order to address the issue of probable contamination in $(Bu_4N)_4SO_4$, we repeated the sensing experiments of the complexes (**1**−**5**) with a fresh lot of $(Bu_4N)_4SO_4$ from a new bottle from Sigma-Aldrich. The results of the sensing experiments are reproducible.
(47) Attempts to determine the binding constants of the complexes for anions with 1/2 stoichiometry did not result in any satisfactory fit. The binding constants were obtained by fitting the data to two successive 1/1 equilibrium processes using eq 1.
(48) Shortreed, M.; Kopelman, R.; Kuhn, M.; Hoyland, B. *Anal. Chem.* **1996**, *68*, 1414.
(49) Ding, Y.; Xie, Y.; Li, X.; Hill, J. P.; Zhang, W.; Zhu, W. *Chem. Commun.* **2011**, *47*, 5431.
(50) Demas, J. N.; DeGraff, B. A. *Anal. Chem.* **1991**, *63*, 829A.
(51) Lakowicz, J. R. *Principles of Fluorescence Spectroscopy*, 2nd ed.; Kluwer Academic/Plenum: New York, 1999.
(52) (a) Kitchen, J. A.; Boyle, E. M.; Gunnlaugsson, T. *Inorg. Chim. Acta* **2012**, *381*, 236. (b) Beer, P. D.; Graydon, A. R.; Sutton, L. R. *Polyhedron* **1996**, *15*, 2457. (c) Duff, T.; Grussing, A.; Thomas, J.-L.; Duati, M.; Vos, J. G. *Polyhedron* **2003**, *22*, 775.
(53) (a) Lin, Z.-H.; Ou, S.-J.; Duan, C.-Y.; Zhang, B.-G.; Bai, Z.-P. *Chem. Commun.* **2006**, 624. (b) Cui, Y.; Niu, Y.-L.; Cao, M. L.; Wang, K.; Mo, H.-J.; Zhong, Y.-R.; Ye, B.-H. *Inorg. Chem.* **2008**, *47*, 5616. (c) Evans, L. S.; Gale, P. A.; Light, M. E.; Quesada, R. *Chem. Commun.* **2006**, 965.
(54) Ireland, J. F.; Wyatt, P. A. *Adv. Phys. Org. Chem.* **1976**, *12*, 131−160.
(55) Montalti, M.; Wadhwa, S.; Kim, W. Y.; Kipp, R. A.; Schmehl, R. H. *Inorg. Chem.* **2000**, *39*, 76−84.
(56) Giordano, P. J.; Bock, C. R.; Wrighton, M. S. *J. Am. Chem. Soc.* **1978**, *100*, 6960−6965.
(57) Hicks, C.; Ye, G.; Levi, C.; Gonzales, M.; Rutenburg, I.; Fan, J.; Helmy, R.; Kassis, A.; Gafney, H. D. *Coord. Chem. Rev.* **2001**, *211*, 207−222.

(58) (a) Dolberg, C. L.; Turo, C. *Inorg. Chem.* **2001**, *40*, 2484−2485. (b) Nazeeruddin, Md. K.; Kalyanasundaram, K. *Inorg. Chem.* **1989**, *28*, 4251−4259. (c) Higgins, B.; DeGraff, B. A.; Demas, J. N. *Inorg. Chem.* **2005**, *44*, 6662−6669. (d) Zheng, G. Y.; Wang, Y.; Rillema, D. P. *Inorg. Chem.* **1996**, *35*, 7118−7123.

(59) (a) Kang, S. O.; Powell, D.; Day, V. W.; Bowman-James, K. *Angew. Chem., Int. Ed.* **2006**, *45*, 7882. (b) Gunnlaugasson, T.; Kruger, P. E.; Jensen, P.; Tierney, J.; Ali, H. D. P.; Hussey, G. M. *J. Org. Chem.* **2005**, *70*, 10875. (c) Gomez, D. E.; Fabbrizzi, L.; Liccheli, M. *J. Org. Chem.* **2005**, *70*, 5717. (d) Boiocchi, M.; Boca, L. D.; Gomez, D. E.; Fabbrizzi, L.; Licchelli, M.; Monzani, E. *Chem. Eur. J.* **2005**, *11*, 3097.

(60) (a) Nishiyabu, R.; Anzenbacher, P., Jr. *J. Am. Chem. Soc.* **2005**, *127*, 8270. (b) Aldakov, D.; Palacios, M. A.; Anzenbacher, P. *Chem. Mater.* **2005**, *17*, 5238.